

this we include in Figure 4 three Ni atoms that are not in **1** but that would be present were the ideal hcp Ni crystal to continue¹⁶ We conclude that the interface between the NiSe portion of **1** and the Ni portion of **1** is exactly the six Ni atoms that are common to both.

Note that the Ni-Ni bonds in the central Ni₁₃ unit of the cluster are on average longer than Ni-Ni bonds in elemental Ni. It is more common for the lattice parameters of nanoclusters of extended solids to be smaller than the corresponding values for those solids. This is usually explained by invoking the surface tension of the solid generating a "Laplace pressure" which compresses the cluster to give shorter internal bond distances. The equivalent chemical explanation is that the otherwise unsatisfied valences on the surface of the cluster are satisfied by surface reconstructions which cause compression of the internal lattice. In the case of **1** the bonding sites external to the Ni₁₃ core are satisfied by the NiSe cap (in addition to the three Se1 atoms and three phosphine ligands which cap the bottom of the cluster), thus the compression of the Ni₁₃ core to a density higher than that of Ni is avoided. In other words, the lattice matching between the Ni core and the NiSe shell force a net expansion of the internal Ni lattice.

The cluster **1** shows structural features of both NiSe and Ni, while the solid-state products of its thermolysis include Ni₃Se₂ and not NiSe. The path by which **1** disproportionates to give the

observed solids presumably, although not necessarily, involves the interdiffusion of the two halves of **1**. The details of the disproportionation are certainly quite complicated and merit further study. Of similar complexity is the route by which **1** is formed from Ni and Se. It is interesting to speculate whether **1** is formed by the fusion of the "Ni-half" and the "NiSe-Half" or by the assembly of some other different sets of atoms or fragments.

Conclusions

We have shown that Ni(COD)₂ reacts with SePEt₃ at elevated temperature to give a mixture of Ni₂Se₂ and Ni, that the two combine at lower temperature to give the cluster **1**, and that **1** gives a similar mixture of Ni₃Se₂ and Ni on heating. We have determined the structure of **1** and analyzed it in terms of associated extended solids, showing it to be a molecular example of an intergrowth of NiSe and Ni. We have characterized the interface between the two members of the intergrowth, showing that interface to be six Ni atoms which are included in both the NiSe and Ni substructures.

Supplementary Material Available: Positional parameters for **1** (Table S1), thermal parameters for **1** (Table S2), complete list of interatomic distances and angles for **1** (Table S3), crystallographic data for inclusion of C atoms (Table S5), positional parameters for **1** including located C atoms (Table S6), and thermal parameters for **1** including located C atoms (Table S7) (11 pages); table of observed and calculated structure factors (Table S4) (55 pages). Ordering information is given on any current masthead page.

(16) The layered description of the Ni₁₉ core of **1** is similar to that shown by Teo and co-workers for Au- and Ag-based clusters: Teo, B. K.; Zhang, H.; Shi, X. *J. Am. Chem. Soc.* 1990, 112, 8552.

Calculation and Electronic Description of Quadratic Hyperpolarizabilities. Toward a Molecular Understanding of NLO Responses in Organotransition Metal Chromophores

David R. Kanis, Mark A. Ratner,* and Tobin J. Marks*

Contribution from the Department of Chemistry and Materials Research Center, Northwestern University, Evanston, Illinois 60208-3113. Received May 18, 1992

Abstract: This contribution explores the use of the computationally efficient, chemically-oriented INDO electronic structure model (ZINDO) in concert with perturbation theory to relate molecular quadratic hyperpolarizabilities to molecular architecture and electronic structure in transition metal chromophores. The ZINDO-derived second-order nonlinear optical responses are found to be in excellent agreement with the experiment for a variety of ferrocenyl and (arene)chromium tricarbonyl derivatives. The assumptions needed to describe nonlinear optical response in simple molecular orbital terms are presented, and their reliability is analyzed in a quantitative fashion. All of the ferrocenyl chromophores examined are found to closely resemble traditional organic π -electron chromophores in that intense MLCT transitions dominate the second-order response. A detailed examination of the modest second-order nonlinearities of the chromium arenes identifies two shortcomings that may be characteristic of many organometallic architectures: the intrinsic hyperpolarizability may be far greater than the experimentally accessible vectorial component of β (that directed along the dipole moment direction), and the electronic distribution about the metal centers in many organometallic structures is pseudo-centrosymmetric. This explains the relatively low nonlinearities of a number of recently reported organometallic chromophores. The design utility of the present computational formalism is illustrated by the calculation of the second-order response of a hypothetical organometallic chromophore having a very acentric electron distribution and, correspondingly, a larger calculated second-order response than any measured to date for an organometallic chromophore.

Introduction

Substances that exhibit highly nonlinear optical (NLO) responses are currently of great scientific and technological interest.¹ While inorganic solids such as LiNbO₃ and KH₂PO₄ have traditionally been the NLO materials of widest interest, recent results suggest that molecule-based macroscopic π -electron ensembles possess many superior NLO characteristics. Specifically, molecule-based NLO materials offer ultrafast response times, lower

dielectric constants, better processability characteristics (e.g., amenability to thin-film fabrication), and enhanced nonresonant NLO responses relative to the traditional inorganic solids.² Since

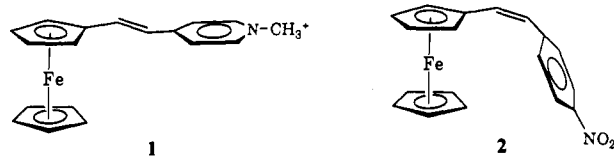
(1) (a) Boyd, R. W. *Nonlinear Optics*; Academic Press: New York, 1992. (b) Prasad, N. P.; Williams, D. J. *Introduction to Nonlinear Optical Effects in Molecules and Polymers*; Wiley: New York, 1991. (c) Eaton, D. F. *Science* 1991, 253, 281-287. (d) Marder, S. R.; Beratan, D. N.; Cheng, L.-T. *Science* 1991, 252, 103-106. (e) Heeger, A. J.; Orenstein, J.; Ulrich, D. R., Eds. *Nonlinear Optical Properties of Polymers*. *Mater. Res. Soc. Symp. Proc.* 1988, 109. (f) Zyss, J. *J. Mol. Electron.* 1985, 1, 25-56. (g) Williams, D. *J. Angew. Chem., Int. Ed. Engl.* 1984, 23, 690-703. (h) Shen, Y. R. *The Principles of Nonlinear Optics*; Wiley: New York, 1984.

* Authors to whom correspondence should be addressed at the Department of Chemistry.

the macroscopic nonlinear optical susceptibility of these molecule-based materials is ultimately governed by the nonlinear optical characteristics of the constituent molecular chromophores, the search for novel molecules displaying optimal nonlinear optical properties is currently an intense area of research in both academia and industry.

Organometallic structures are intriguing candidates for study as NLO chromophores by virtue of their low-energy, yet sometimes intense, electronic transitions.³ Such linear optical characteristics are suggestive signatures of molecules exhibiting significant nonlinear optical response.² In addition, coordinating a ligand containing highly polarizable π -electrons to a metallic center having weakly bound valence electrons (i.e., which is highly polarizable) could, in principle, yield electronic structures that exhibit enhanced optical nonlinearities. The great structural and electronic diversity available in metal-organic environments could furthermore introduce into chromophore design strategies a host of new tunable parameters not available in simple π -organic structures. Finally, organometallic subunits, by virtue of the large number of available coordination sites about a metal center, could conceivably be incorporated into macroscopic matrices through a variety of novel attachment schemes.

Several reports have appeared in the recent literature quoting appreciable macroscopic second-order nonlinear optical susceptibilities for powders of transition-metal organometallic chromophores.⁴⁻⁶ Two molecules, *trans*-1-ferrocenyl-2-(*N*-methylpyridinium-4-yl)ethylene iodide⁶ (1) and *cis*-1-ferrocenyl-2-(4-nitrophenyl)ethylene⁵ (2), were reported to possess rather large powder nonlinearities (220 and 62 \times urea, respectively) and have sparked subsequent research activity in this area. However, in striking contrast to conventional organic systems, neither a chemically oriented rationalization of nor a quantitative quantum



chemical prescription for optimal responses in organometallic structures is currently available. Moreover, despite intense research efforts in this area, all microscopic second-order nonlinear responses (β_{vec}) reported for organometallic chromophores to date are considerably less than those of their π -electron organic counterparts.^{7,8}

In this contribution, we report the first theoretical investigation of organometallic structures as second-order nonlinear optical chromophores using the accurate, chemically oriented, computationally efficient ZINDO-SOS quantum chemical formalism. By comparing computed quadratic hyperpolarizabilities with recent organometallic solution phase DC electric field-induced second harmonic generation (EFISH) data,^{7,8} we are able to demonstrate the reliability of this approach, rationalize known molecular responses, suggest chemical modifications that should lead to greater nonresonant second-order susceptibilities, and put forth general prescriptions for optimizing the β tensor in metal-containing chromophoric structures. The representative classes of organometallic chromophores examined in this work will be the derivatized ferrocenyl molecules and the modified (arene)chromium tricarbonyl complexes.

One can envision four generic classes of transition-metal organometallic architectures which could, in principle, yield enhanced second-order nonlinear optical responses. They are (1) structures possessing spectroscopically intense metal-to-ligand charge-transfer (MLCT) or (2) ligand-to-metal charge-transfer (LMCT) excitations, (3) organometallic or classic Werner type complexes where the metal atom(s) act(s) as an intermediary between an electron donor and an electron acceptor moiety, and (4) molecules which do not fit within the usual criteria for enhanced responses in nonlinear optical templates. In this contribution, we discuss the fundamental principles associated with exploiting MLCT bands in organometallic chromophores. This class of chromophores has been the most widely studied of the four and arguably offers the greatest promise for incorporation into $\chi^{(2)}$ materials. Future contributions will address the electronic origin of the second-order response for classes 2-4.

The underlying rationale for exploiting MLCT bands in frequency doubling is simple to understand. If an isolated ligand possessed a strong π to π^* charge-transfer transition, linking a metal fragment to the ligand π -network might introduce an optical charge-transfer transition from a "nonbonding" metal-based state to the ligand-based π^* -state. As shown schematically in Figure 1, the energy of the MLCT band is expected to be at lower energy than that of the predominant π to π^* transition in the isolated ligand. Researchers have long recognized the importance of having low-lying charge-transfer states for optimizing nonresonant nonlinear optical responses.² Therefore, it should, in principle, be possible to design metal-organic architectures possessing enhanced nonresonant second-order responses relative to those of uncoordinated organic moieties.

Computational Details

A quantitative description of molecular nonlinear optical response is derived from a power series expansion of the molecular dipole moment (polarization) upon interaction with an oscillating external electromagnetic field (eq 1).¹

$$p_i = \sum_j \alpha_{ij} E_j + \sum_{j \geq k} \beta_{ijk} E_j E_k + \sum_{j \geq k \geq l} \gamma_{ijkl} E_j E_k E_l + \dots \quad (1)$$

Here p_i is the molecular polarization induced along the i th axis, E_j is the j th component of the applied electric field, α is the linear polarizability,

(2) (a) Marder, S. R.; Sohn, J. E.; Stucky, G. D., Eds. *Materials for Nonlinear Optics: Chemical Perspectives*; ACS Symposium Series 455; American Chemical Society: Washington, DC, 1991. (b) Khanarian, G., Ed. *Nonlinear Opt. Prop. Org. Mater. III; Proc. SPIE-Int. Soc. Opt. Eng.* **1990**, 1337. (c) Khanarian, G., Ed. *Nonlinear Opt. Prop. Org. Mater. II; Proc. SPIE-Int. Soc. Opt. Eng.* **1990**, 1147. (d) Hann, R. A.; Bloor, D., Eds. *Organic Materials for Nonlinear Optics*; Royal Society of Chemistry Monograph 69; Burlington House: London, 1988. (e) Chemla, D. S.; Zyss, J., Eds. *Nonlinear Optical Properties of Organic Molecules and Crystals*; Academic Press: New York, 1987; Vols. 1 and 2. (f) Williams, D. J., Ed. *Nonlinear Optical Properties of Organic Molecules and Polymeric Materials*; ACS Symposium Series 233; American Chemical Society: Washington, DC, 1984.

(3) See, for example: (a) Lever, A. B. P. *Inorganic Electronic Spectroscopy*, 2nd ed.; Elsevier: Amsterdam, 1984; Chapter 5. (b) Geoffroy, G. L.; Wrighton, M. S. *Organometallic Photochemistry*; Academic Press: New York, 1979; Chapter 1.

(4) (a) Kimura, M.; Abel-Halim, H.; Robinson, D. W.; Cowan, D. O. *J. Organomet. Chem.* **1991**, *403*, 365-372. (b) Pollagi, T. P.; Stoner, T. C.; Dallinger, R. F.; Gilbert, T. M.; Hopkins, M. D. *J. Am. Chem. Soc.* **1991**, *113*, 703-704. (c) Coe, B. J.; Jones, C. J.; McCleverty, J. A.; Bloor, D.; Kolinsky, P. V.; Jones, R. J. *J. Chem. Soc., Chem. Commun.* **1989**, 1485-1487. (d) Tam, W.; Calabrese, J. C. *Chem. Phys. Lett.* **1988**, *144*, 79-82. (e) Bandy, J. A.; Bunting, H. E.; Garcia, M. H.; Green, M. L. H.; Marder, S. R.; Thompson, M. E.; Bloor, D.; Kolinsky, P. V.; Jones, R. J. In ref 2d, pp 225-231. (f) Eaton, D. F.; Anderson, A. G.; Tam, W.; Wang, Y. *J. Am. Chem. Soc.* **1987**, *109*, 1886-1888. (g) Calabrese, J. C.; Tam, W. *Chem. Phys. Lett.* **1987**, *133*, 244-245. (h) Anderson, A. G.; Calabrese, J. C.; Tam, W.; Williams, I. D. *Chem. Phys. Lett.* **1987**, *134*, 392-396. (i) Frazier, C. C.; Harvey, M. A.; Cockerham, M. P.; Hand, H. M.; Chaudard, E. A.; Lee, C. H. *J. Phys. Chem.* **1986**, *90*, 5703-5706. (j) Lamberth, C.; Murphy, D. M.; Mingos, D. M. P. *Spec. Publ. - R. Soc. Chem.* **1991**, *91* (Org. Mater. Non-Linear Opt. 2), 183-189. (k) Lesley, G.; Yuan, Z.; Stringer, G.; Jobe, I. R.; Taylor, N. J.; Koch, L.; Scott, K.; Marder, T. B.; Williams, I. D.; Kurtz, S. K. *Spec. Publ. - R. Soc. Chem.* **1991**, *91* (Org. Mater. Non-Linear Opt. 2), 197-203. (l) Chiang, W.; Thompson, M. E.; Van Engen, D. *Spec. Publ. - R. Soc. Chem.* **1991**, *91* (Org. Mater. Non-Linear Opt. 2), 210-216. (m) Nalwa, H. S. *Appl. Organomet. Chem.* **1991**, *5*, 349-377. (n) Zhang, N.; Jiang, M. H.; Yuan, D. R.; Xu, D.; Tao, X. T.; Shao, Z. S. *J. Cryst. Growth* **1990**, *102*, 581-584. (o) Tao, X.; Zhang, N.; Yuan, D.; Xu, D.; Yu, W.; Jiang, M. In ref 2d, pp 385-389. (p) Sakaguchi, H.; Nagamura, T.; Matsuo, T. *Jpn. J. Appl. Phys.* **1991**, *30*, L377-L379. (q) Richardson, T.; Roberts, G. G.; Polywka, M. E. C.; Davies, S. G. *Thin Solid Films* **1989**, *179*, 405-411.

(5) Green, M. L. H.; Marder, S. R.; Thompson, M. E.; Bandy, J. A.; Bloor, D.; Kolinsky, P. V.; Jones, R. J. *Nature* **1987**, *330*, 360-362.

(6) Marder, S. R.; Perry, J. W.; Schaefer, W. P.; Tiemann, B. G.; Groves, P. C.; Perry, K. In ref 2c, 108-115.

(7) Cheng, L.-T.; Tam, W.; Meredith, G. R.; Marder, S. R. *Mol. Cryst. Liq. Cryst.* **1990**, *189*, 137-153.

(8) Calabrese, J. C.; Cheng, L.-T.; Green, J. C.; Marder, S. R.; Tam, W. *J. Am. Chem. Soc.* **1991**, *113*, 7227-7232.

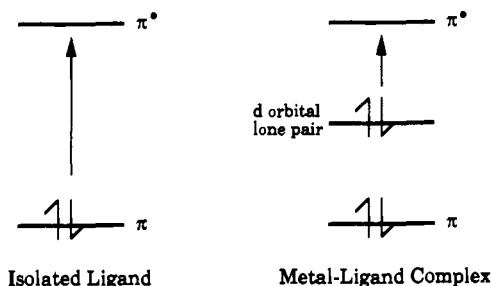


Figure 1. Schematic representation depicting the predicted effect on optical transitions of appending a metal fragment to an organic ligand.

β , the quadratic hyperpolarizability, and γ , the cubic hyperpolarizability. α , β , and γ describe the responsivity of the molecule to an electromagnetic perturbation and are constants for a given molecular geometry. The β tensor is responsible for second-harmonic generation (SHG) and is the quantity of interest in this work.

Several theoretical approaches for accurately calculating β tensors have appeared in the literature. Computationally intensive methods such as coupled Hartree-Fock,⁹ derivative Hartree-Fock,¹⁰ and correlated wave¹¹ ab initio procedures are presently applicable to molecules of only limited size. The number of valence electrons in the chromophoric structures examined herein and the current lack of suitable extended transition-metal basis sets prohibit employing any of these rigorous treatments in the present study. Rather, the structurally elaborate chromophores of interest here will be treated within a perturbative framework where the electronic states mixed by the laser field are expressed as a sum over excited particle-hole states (SOS). Since the nonlinear optical expansion coefficients are functions of linear optical properties such as excitation energies and dipole matrix elements, the necessary electronic structure information can be conveniently obtained from a spectroscopically based semiempirical electronic structure description. Indeed, previous sum-over-states studies have employed either a modified all-valence CNDO/S¹² (Complete Neglect of Differential Overlap), a π -electron PPP¹³ (Parr-Pariser-Pople), or, more recently, an all-valence INDO/S¹⁴⁻¹⁶ (Intermediate Neglect of Differential Overlap) formalism to compute frequency-doubling efficiencies. These computationally efficient, chemically oriented quantum chemical methods have been remarkably successful at both predicting and rationalizing observed nonlinear optical responses for π -electron organic chromophores. Here we employ, for the first time, the transition-metal INDO/S formalism (ZINDO)¹⁷ to describe the second-order NLO response of transition-metal-containing chromophores.

(9) (a) Karna, S. P.; Prasad, P. N.; Dupuis, M. *J. Chem. Phys.* **1991**, *94*, 1171-1181. (b) Meyers, F.; Adant, C.; Bredás, J. L. *J. Am. Chem. Soc.* **1991**, *113*, 3715-3719. (c) Caves, T. C.; Karplus, M. *J. J. Chem. Phys.* **1969**, *50*, 3649-3661.

(10) Dykstra, C. E.; Jasien, P. J. *J. Chem. Phys. Lett.* **1984**, *109*, 388-393.

(11) (a) Sekino, H.; Bartlett, R. J. *J. Chem. Phys.* **1991**, *94*, 3665-3669. (b) Rice, J. E.; Amos, R. D.; Colwell, S. M.; Handy, N. C.; Sanz, J. *J. Chem. Phys.* **1990**, *93*, 8828-8839. (c) Sekino, H.; Bartlett, R. J. *J. Chem. Phys.* **1986**, *85*, 976-989. (d) Subbaswamy, K. R.; Mahan, G. D. *J. Chem. Phys.* **1986**, *84*, 3317-3319.

(12) (a) Morley, J. O. *J. Am. Chem. Soc.* **1988**, *110*, 7660-7663. (b) Docherty, V. J.; Pugh, D.; Morley, J. O. *J. Chem. Soc., Faraday Trans. 2* **1985**, *81*, 1179-1192. (c) Garito, A. F.; Teng, C. C.; Wong, K. Y.; Emankahamiri, O. *Mol. Cryst. Liq. Cryst.* **1984**, *106*, 219-258. (d) Lalama, S. L.; Garito, A. F. *Phys. Rev.* **1979**, *20*, 1179-1194. (e) Morrell, J. A.; Albrecht, A. C. *J. Chem. Phys. Lett.* **1979**, *64*, 46-50.

(13) (a) Li, D.; Ratner, M. A.; Marks, T. J. *J. Phys. Chem.* **1992**, *96*, 4325-4336. (b) Soos, Z. G.; Ramasesha, S. *J. Chem. Phys.* **1989**, *90*, 1067-1076. (c) de Melo, C. P.; Silbey, R. *J. Chem. Phys.* **1988**, *88*, 2567-2566. (d) Li, D.; Marks, T. J.; Ratner, M. A. *J. Am. Chem. Soc.* **1988**, *110*, 1707-1715. (e) Li, D.; Marks, T. J.; Ratner, M. A. *J. Chem. Phys. Lett.* **1986**, *131*, 370-375. (f) Dirk, C. W.; Twieg, R. J.; Wagniere, G. *J. Am. Chem. Soc.* **1986**, *108*, 5387-5395.

(14) (a) Kanis, D. R.; Ratner, M. A.; Marks, T. J.; Zerner, M. C. *Chem. Mater.* **1991**, *3*, 19-22. (b) Kanis, D. R.; Ratner, M. A.; Marks, T. J. *J. Am. Chem. Soc.* **1990**, *112*, 8203-8204. (c) Ulman, A.; Willand, C. S.; Kohler, W.; Robello, D. R.; Williams, D. J.; Handley, L. *J. Am. Chem. Soc.* **1990**, *112*, 7083-7090. (d) Ulman, A. *J. Phys. Chem.* **1988**, *92*, 2385-2390. (e) Parkinson, W. A.; Zerner, M. C. *J. Chem. Phys.* **1989**, *90*, 5606-5611.

(15) A coupled Hartree-Fock study incorporating an INDO Hamiltonian has been carried out on classical organic chromophores. *Zyss, J. J. Chem. Phys.* **1979**, *70*, 3333-3340.

(16) Kanis, D. R.; Marks, T. J.; Ratner, M. A. *Int. J. Quantum Chem.* **1992**, *43*, 61-82.

(17) Anderson, W. P.; Edwards, W. D.; Zerner, M. C. *Inorg. Chem.* **1986**, *25*, 2728-2732.

In the SOS treatment employed in this study, the ground state is taken as the Hartree-Fock single determinant, and the electronic states created by the perturbing laser field are treated as an infinite sum over unperturbed particle-hole states, where the individual components of the quadratic hyperpolarizability are given by eq 2.¹⁸

$$\beta_{ijk} + \beta_{ikj} = -\frac{e^3}{4\hbar^2} \left[\sum_{n \neq g} \sum_{m \neq g} \left\{ (r_{gn}^j r_{nm}^i r_{mg}^k + r_{gn}^k r_{nm}^j r_{mg}^i) \times \left(\frac{1}{(\omega_{ng}^j - \omega)(\omega_{ng}^m + \omega)} + \frac{1}{(\omega_{ng}^j + \omega)(\omega_{ng}^m - \omega)} \right) + (r_{gn}^j r_{nm}^i r_{mg}^k + r_{gn}^k r_{nm}^j r_{mg}^i) \left(\frac{1}{(\omega_{ng}^j + 2\omega)(\omega_{ng}^m + \omega)} + \frac{1}{(\omega_{ng}^j - 2\omega)(\omega_{ng}^m - \omega)} \right) + (r_{gn}^j r_{nm}^i r_{mg}^k + r_{gn}^k r_{nm}^j r_{mg}^i) \left(\frac{1}{(\omega_{ng}^j - \omega)(\omega_{ng}^m - 2\omega)} + \frac{1}{(\omega_{ng}^j + \omega)(\omega_{ng}^m + 2\omega)} \right) \right\} + 4 \sum_{n \neq g} \left\{ [r_{gn}^j r_{ng}^k \Delta r_{ng}^i (\omega_{ng}^2 - 4\omega^2) + r_{gn}^k r_{ng}^i \Delta r_{ng}^j (\omega_{ng}^2 + 2\omega^2)] \frac{1}{(\omega_{ng}^2 - \omega^2)(\omega_{ng}^2 - 4\omega^2)} \right\} \right] \quad (2)$$

Here ω is the frequency of the applied electric field, $r_{in}^j = \langle \psi_n | r^j | \psi_n \rangle$ is the matrix element of the displacement operator $r^{(j)}$ along the i th molecular axis between electronic states ψ_n and ψ_n , $\Delta r_{ng}^j = r_{nn}^j - r_{gg}^j$ is the dipole moment difference between the excited state and ground state (denoted by g), and $\hbar\omega_{ng}$ is the energy separation between the ground-state and an excited-state ψ_n . The transition moment matrix elements are computed in dipole length form using LCAO-MO coefficients and the Pariser approximation¹⁹ for matrix elements over atomic orbitals (eq 3), where R_{λ}^i is a Cartesian coordinate. In this treatment, as in other

$$r_{\lambda\lambda}^i = \delta_{\lambda\lambda} R_{\lambda}^i \quad (3)$$

semiempirical approaches that compute linear and nonlinear optical properties, the monoexcited configuration interaction (MECI) approximation²⁰ is employed to describe the excited states. In principle, all possible monoexcited states should be included in the summation over ψ_n and ψ_n in eq 2; however, it will be seen that the computed second-order response converges without including all possible excited states of the valence basis. In the computations reported here, the 100 lowest energy transitions between SCF electronic configurations were chosen to undergo CI mixing and the resulting 100 states were then summed over in eq 2. The validity of truncating the infinite sum in eq 2 will be established later in this contribution.

Although all 27 components of the β tensor can be computed, only the vector component along the dipole moment direction, β_{vec} (eq 4), is sampled experimentally in electric-field-induced-second-harmonic-generation (EFISH) experiments.²¹

$$\beta_{vec}(-2\omega; \omega, \omega) = \sum_{i=1}^3 \frac{\mu_i \beta_i}{|\mu|} \quad (4)$$

Here, μ is the ground-state molecular dipole moment and

$$\beta_i = \beta_{iii} + \frac{1}{3} \sum_{j \neq i} (\beta_{ijj} + \beta_{jij} + \beta_{jji}) \quad (5)$$

where i and j run over the molecular Cartesian directions x , y , and z .

Another quantity of interest in this work is the total quadratic hyperpolarizability, β_{tot} (eq 6). β_{vec} will be identical to β_{tot} when the charge

$$\beta_{tot} = \sqrt{(\beta_x^2 + \beta_y^2 + \beta_z^2)} \quad (6)$$

transfer is unidirectional and parallel to the molecular dipole moment. Note that β_{tot} is always a positive quantity regardless of the sign of the individual vectorial components. It is conceivable that a molecule could have a large nonlinear optical response, but not along the molecular axis sampled by the EFISH measurement, so that β_{vec} would differ substantially from β_{tot} . This situation might be found in organometallic molecules having MLCT transitions, since the metal orbitals involved in charge transfer are usually significantly "nonbonding" in the ground state

(18) Ward, J. F. *Rev. Mod. Phys.* **1971**, *37*, 1-18.

(19) Pariser, R.; Parr, R. G. *J. Chem. Phys.* **1953**, *21*, 466-471.

(20) Linderberg, J.; Öhrn, Y. *J. Chem. Phys.* **1967**, *49*, 716-727.

(21) Levine, B. F.; Bethea, C. G. *Appl. Phys. Lett.* **1974**, *24*, 445-447.

(i.e., do not appreciably contribute to the ground-state dipole moment).

We compare here our theoretical β_{vec} results to a recently tabulated, internally consistent set of EFISH data.^{7,8} In using EFISH results from a single laboratory, we minimize deviations due to experimental conditions such as differing incident frequencies, solvent polarities, local field models, and data reduction schemes. The EFISH, optical spectral, and dipole moment data quoted in this work were measured in relatively nonpolar solvents and with an incident laser frequency of 1.91 μm ($\hbar\omega = 0.65$ eV).

The ZINDO semiempirical formalism employed in this study has been discussed in detail elsewhere.^{17,22} This computationally efficient scheme provides an accurate, chemically oriented description of linear optical properties for a wide range of transition-metal-containing structures. Molecular integrals are either computed rigorously, neglected, approximated with atomic parameters (ionization potentials, one-center coulomb integrals), or evaluated using a minimal number of well-defined empirical parameters (one parameter per atom). For the present NLO investigation, the ZINDO algorithm was implemented without any parameter manipulation or basis function alteration.^{17,22} All nonlinear optical computations were performed on a Stellar 2000 minisupercomputer, and all molecular NLO computations required less than 30 min of CPU time per molecule.

The geometrical coordinates chosen for the present calculations were based on published crystallographic data. We have previously demonstrated that idealized nuclear coordinates are a legitimate alternative to optimized structures for input in NLO calculations, and all molecular structures in this work were idealized in accord with the prescription reported therein.¹⁶ Bond distances and angles of organic fragments were those given previously,¹⁶ where the bridging polyene structures employed bond-alternating distances of 1.44–1.36–1.44 Å. The ferrocenyl chromophore geometric parameters were based upon the crystal structure of ferrocene,²³ with Fe–C bond distances set at 2.04 Å and cyclopentadienyl C–C distances at 1.40 Å. The cyclopentadienyl stilbene portion of the trans ferrocenyl chromophore was chosen to be planar, while the stilbene fragment in the cis ferrocenyl stilbene analogues (2 and 5) was rotated out of the cyclopentadienyl plane by 30°, in accordance with the crystal structure of 2.⁵ The nuclear coordinates for all Cr(CO)₃-arene structures were based upon the crystal structure of the parent (η^6 -benzene)chromium tricarbonyl chromophore (15).²⁴ The geometry about the metal center was assumed to be octahedral with the Cr–C(arene) distances set at 2.20 Å, the Cr–CO distance, at 1.84 Å, the C–O distance, at 1.15 Å, and all the arene C–C distances fixed at 1.40 Å. The Cr–NH₃ bond lengths employed in the hypothetical structures were taken to be 2.07 Å, as found in a representative tetraamminechromium(III) structure.²⁵

Results and Discussion

Sum over States Truncation. For the present ZINDO-SOS NLO computations, we have chosen to restrict the SOS summation and CI basis set to 100 excited configurations (vide supra). This has proven to be a valid approximation in computing β_{vec} for archetypical donor-acceptor π -electron organic chromophores.¹⁶ For example, in Figure 2a, the computed nonresonant second-order response for the prototypical organic chromophore, 4-amino-4'-nitrostilbene, is plotted versus basis set size. The second-order β_{vec} response reaches a converged value, which is in good agreement with the EFISH-determined response, with less than 50 excited states. Since the salient features of this plot are representative of those found for all π -organic chromophores examined to date,¹⁶ we now assume that a basis set size of 100 is sufficient for all second-order susceptibility calculations on conventional push-pull organic chromophores of similar molecular dimensions.

In the case of transition-metal complexes, a significant number of "NLO inactive" ligand field (d-to-d) transitions occur at a lower energy than the "NLO active" MLCT transitions. Therefore, one might anticipate that a relatively large CI basis set would be necessary to collect all of the β -determining charge-transfer

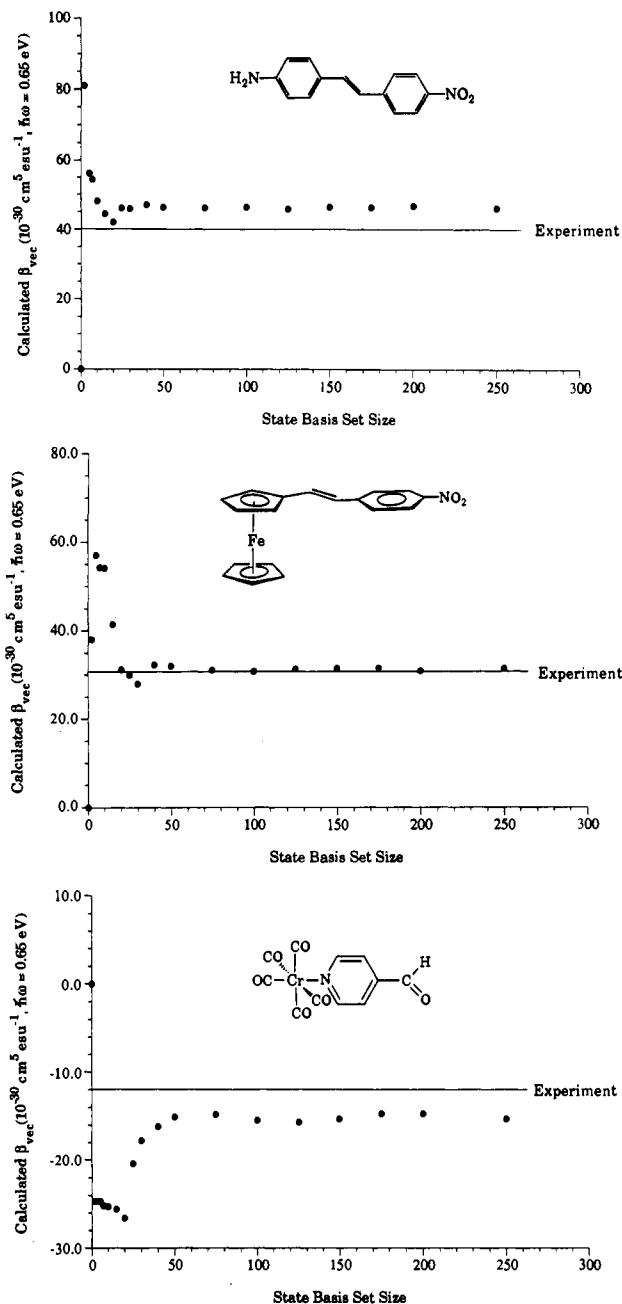


Figure 2. Plots of ZINDO-derived β_{vec} as a function of the number of state basis functions included in both configuration interaction and sum-over-states expansion for (a, top) 4-amino-4'-nitrostilbene, (b, middle) trans-1-ferrocenyl-2-(4-nitrophenyl)ethylene, and (c, bottom) (4-formylpyridinyl)chromium pentacarbonyl.

transitions. As shown in Figures 2b,c, however, the calculated β response for two representative organometallic chromophores converges far below the 100 state size chosen for these studies. The approach to convergence of the organometallic curves is, however, slightly less steep than that for the stilbene derivative, suggesting that a slightly larger basis set is required for accurately describing β_{vec} for organometallics than for organics. Nevertheless, the ZINDO-derived quadratic hyperpolarizabilities for these two representative organometallic chromophores converge well before the chosen basis set of size of 100.

Since the calculated quadratic hyperpolarizability for the (pyridine)Cr(CO)₃ derivative is negative, the basis set convergence plot (Figure 2c) is a mirror image of those for the two positive- β -chromophores (Figure 2a,b). The computed signs of the second-order responses are in agreement with experiment;⁷ a qualitative rationale for these sign differences will be discussed in a subsequent contribution.²⁷

(22) (a) Anderson, W. P.; Cundari, T. R.; Drago, R. S.; Zerner, M. C. *Inorg. Chem.* **1990**, *29*, 1–3. (b) Zerner, M. C.; Loew, G. H.; Kirchner, R. F.; Mueller-Westerhoff, U. T. *J. Am. Chem. Soc.* **1980**, *102*, 589–599. (c) Bacon, A. D.; Zerner, M. C. *Theor. Chim. Acta (Berlin)* **1979**, *53*, 21–54. (d) Ridley, J.; Zerner, M. C. *Theor. Chim. Acta (Berlin)* **1973**, *32*, 111–134.

(23) (a) Takusagawa, F.; Koetzle, T. F. *Acta Crystallogr., Sect. B* **1979**, *35*, 1074–1081. (b) Dunitz, J. D.; Orgel, L. E.; Rich, A. *Acta Crystallogr.* **1956**, *9*, 373–375.

(24) Bailey, M. F.; Dahl, L. F. *Inorg. Chem.* **1965**, *4*, 1314–1319.

(25) Chang, J. C.; Gerdorn, L. E.; Baenziger, N. C.; Goff, H. M. *Inorg. Chem.* **1983**, *22*, 1739–1744.

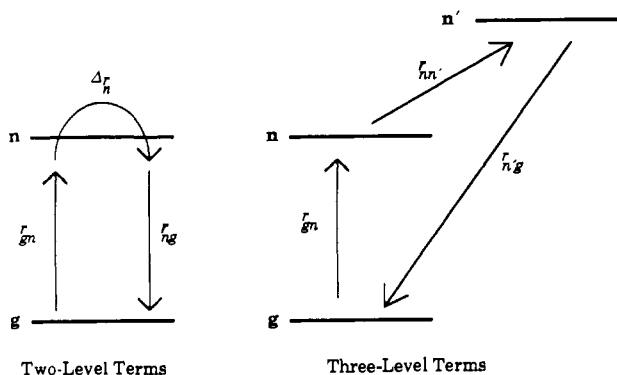


Figure 3. Diagrammatic representations of the two-level and three-level contributions to the second-order susceptibility.

Relative Importance of Three-Level Terms versus Two-Level Terms in the SOS Treatment of Nonlinear Optical Response. It is somewhat surprising that the salient features of Figure 2b,c strongly resemble those observed for the 4-amino-4'-nitrostilbene in Figure 2a. In fact, of the many hundreds of NLO chromophores investigated to date in this laboratory with the ZINDO-SOS method (organic and organometallic), only a handful do not possess a basis set curve with a distinctive maximum followed by a steep decline to approximately half the maximum value at convergence. To rationalize NLO responses in terms of chemically based electronic structure arguments, we must briefly comment on several general features of these plots.²⁷ This discussion requires that we decompose the SOS prescription for computing β (eq 2) into two components, $\beta_{\text{vec},2}$ and $\beta_{\text{vec},3}$.

We can partition the sum-over-states expression (eq 2) into two contributions, a so-called two-level term (eq 7, $\beta_{ijk,2}$) and a three-level term (eq 8, $\beta_{ijk,3}$). The algorithms for converting the

$$\beta_{ijk,2} = -\frac{e^3}{2\hbar^2} \sum_{n \neq g} \left\{ [r_{gn}^j r_{gn}^k \Delta_n^i (\omega_{ng}^2 - 4\omega^2) + r_{gn}^j r_{gn}^k \Delta_n^i] \frac{1}{(\omega_{ng}^2 - \omega^2)(\omega_{ng}^2 - 4\omega^2)} \right\} \quad (7)$$

$$\beta_{ijk,3} = -\frac{e^3}{8\hbar^2} \sum_{n \neq g} \sum_{n' \neq n} \left\{ (r_{gn}^j r_{n'n}^i r_{n'g}^k + r_{gn}^k r_{n'n}^i r_{n'g}^j) \times \left(\frac{1}{(\omega_{n'g} - \omega)(\omega_{ng} + \omega)} + \frac{1}{(\omega_{n'g} + \omega)(\omega_{ng} - \omega)} \right) + (r_{gn}^j r_{n'n}^i r_{n'g}^k + r_{gn}^k r_{n'n}^i r_{n'g}^j) \left(\frac{1}{(\omega_{n'g} + 2\omega)(\omega_{ng} + \omega)} + \frac{1}{(\omega_{n'g} - 2\omega)(\omega_{ng} - \omega)} \right) + (r_{gn}^j r_{n'n}^i r_{n'g}^k + r_{gn}^k r_{n'n}^i r_{n'g}^j) \times \left(\frac{1}{(\omega_{n'g} - \omega)(\omega_{ng} - 2\omega)} + \frac{1}{(\omega_{n'g} + \omega)(\omega_{ng} + 2\omega)} \right) \right\} \quad (8)$$

27 individual tensorial elements into components along the ground-state dipole moment direction ($\beta_{\text{vec},2}$ and $\beta_{\text{vec},3}$) are given by eqs 4 and 5. Ultimately, eq 9 is obtained.

$$\beta_{\text{vec}} = \beta_{\text{vec},2} + \beta_{\text{vec},3} \quad (9)$$

Each two-level component in the infinite sum for $\beta_{ijk,2}$ (eq 7) contains only two states, the ground state, g , and one excited state, n . As shown by the diagrammatic representation of the two-level process (Figure 3), the first photon couples n with the ground state through r_{gn} , the second photon mixes n with itself via Δ_n and

the third couples n with g through r_{ng} . Fortunately, the complex mathematical description of the two-level contributions can be expressed in terms of the familiar quantities f_{gn} (oscillator strength of a transition from g to n), $\hbar\omega_{gn}$ (energy difference between g and n), and $\Delta\mu_{gn}$ (difference in dipole moments between n and g). If the summation in eq 7 is limited to one dominant transition and charge-transfer is unidirectional, as is usually the case for typical organic chromophores, the classic two-level model originally proposed by Oudar is obtained (eq 10).²⁸

$$\beta_{\text{Oudar}} = \frac{3e^2}{2} \frac{\hbar\omega_{gn} f_{gn} \Delta\mu_{gn}}{[(\hbar\omega_{gn})^2 - (2\hbar\omega)^2][(\hbar\omega_{gn})^2 - (\hbar\omega)^2]} \quad (10)$$

The three-level contributions in the SOS formalism (eq 8) contain a ground state and *two* excited states, n and n' . The first photon couples g with n through r_{gn} , the second photon mixes n and n' through $r_{nn'}$, and the third connects n' with g via $r_{n'g}$ (Figure 3). Since detailed information on excited state-to-excited state (i.e. two-photon) transitions ($r_{nn'}$) is not currently available for most chemical systems, a qualitative, chemically-oriented description of these complex three-level mathematical expressions is not immediately evident.

One might naively assume that the magnitude of $\beta_{\text{vec},3}$ is significantly less than that of $\beta_{\text{vec},2}$. Most chromophoric structures possess only one highly allowed electronic transition in the visible or near-UV spectral region; that is, if r_{gn} is large, $r_{n'g}$ must necessarily be small. The product of $r_{gn} r_{nn'} r_{n'g}$ (generic three-level expression) should then be significantly less than $r_{gn} \Delta_n r_{ng}$ (generic two-level expression) for most nonlinear chromophoric structures. However, a ZINDO-SOS analysis reveals that many n' states can efficiently couple to a given n through large $r_{nn'}$ integrals. Thus, many large $r_{nn'}$ values for a given excited state n could potentially overcome the relatively small values of $r_{n'g}$ to allow $\beta_{\text{vec},3}$ to compete effectively with the one or two dominant terms in $\beta_{\text{vec},2}$. Our computations suggest, therefore, that the three-level contributions cannot a priori be ignored when describing NLO responses with the ZINDO-SOS formalism.²⁷

Returning to the basis set curves in Figure 2, we can now rationalize the characteristic shapes of these plots. In all three molecules, one excited state (n) is responsible for the observed maximum early in the summation. When additional states are included in the NLO calculations, the computed response shows a *marked decrease* in sharp disagreement with the simple two-level model. We note that the general features of the basis set plots for these three chromophores are not unique to this work.^{14c,29} While such a decline has been noted previously, no explanation for this curious effect has been advanced. Our analysis reveals that the marked decrease in β is due to many three-level contributions rather than to additional two-level mechanisms. For most of the chromophores we have examined to date, all three-level terms are of opposite sign from the dominant two-level contribution. As shown in Figure 2, a number of excited states are involved in decreasing the observed response to the converged value via a three-level process. Clearly, the three-level contributions are important in describing the origin of the second-order response in these chromophores.

Since the three-level terms are non-negligible in these β_{vec} results and since there is no chemically oriented model available to rationalize the $\beta_{\text{vec},3}$ contributions, how then can we rationalize the β_{vec} values in familiar chemical terms? The empirical answer lies in the relative magnitudes of the three-level versus two-level contributions. The *sum of the three-level terms is found to scale approximately as the sum of the two-level terms in nearly all organic and organometallic molecules examined to date*. Specifically, the three-level terms reduce β_{vec} by approximately half the value of $\beta_{\text{vec},2}$.³⁰ We propose, therefore, that a qualitative description of the nonlinear optical response can be gleaned from

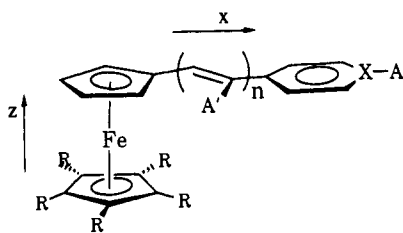
(26) For the chromium-pyridine complex, the ZINDO β_{vec} value is compared with an EFISH β_{vec}^7 for the analogous tungsten derivative. This replacement was necessary due to the present computational limitations of the ZINDO procedure.

(27) We are preparing a manuscript that will discuss this aspect of the NLO computations in greater detail.

(28) (a) Oudar, J. L. *J. Chem. Phys.* **1977**, *67*, 446-457. (b) Oudar, J. L.; Chemla, D. S. *J. Chem. Phys.* **1977**, *66*, 2664-2668.

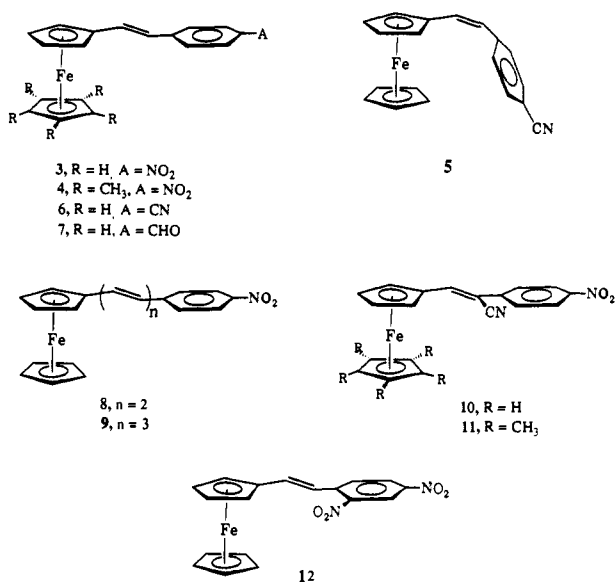
(29) Pugh, D.; Morley, J. O. In ref 2e.

(30) Perturbation-theoretic analysis rationalizes this behavior. Kanis, D. R.; Marks, T. J.; Ratner, M. A. Manuscript in preparation.

Table I. Comparison of Experimental and ZINDO-Derived Molecular Hyperpolarizabilities along the Dipole Moment Direction (β_{vec}) and the ZINDO-Derived Total Intrinsic Hyperpolarizability (β_{tot}) at 1.91 μm ($\hbar\omega = 0.65$ eV) for a Series of Ferrocenyl Derivatives^a


| | X-A | R | A' | n | isomer | $\beta_{\text{vec}}^{\text{expt } b}$ | $\beta_{\text{vec}}^{\text{calc}}$ | $\beta_{\text{tot}}^{\text{calc}}$ | μ_x^{calc} | μ_y^{calc} | μ_z^{calc} | $\mu^{\text{expt } b}$ |
|----|---------------------------------------|-----------------|----|---|--------|---------------------------------------|------------------------------------|------------------------------------|-----------------------|-----------------------|-----------------------|------------------------|
| 1 | N-CH ₃ ⁺ | H | H | 1 | E | | 67.6 | 68.9 | | | | |
| 2 | C-NO ₂ | H | H | 1 | Z | 13 | 20.7 | 21.0 | -1.0 | -7.4 | -0.3 | 4.0 |
| 3 | C-NO ₂ | H | H | 1 | E | 31 | 30.8 | 30.8 | -8.8 | -0.5 | -0.3 | 4.5 |
| 4 | C-NO ₂ | CH ₃ | H | 1 | E | 40 | 34.7 | 34.7 | -8.2 | -0.5 | -0.7 | 4.4 |
| 5 | C-CN | H | H | 1 | Z | 4.0 | 5.49 | 5.92 | -0.6 | -5.4 | -0.2 | 3.9 |
| 6 | C-CN | H | H | 1 | E | 10 | 9.72 | 9.76 | -5.8 | -0.4 | -0.2 | 4.6 |
| 7 | C-CHO | H | H | 1 | E | 12 | 15.1 | 17.2 | -4.4 | -3.5 | -0.2 | 3.9 |
| 8 | C-NO ₂ | H | H | 2 | E,E | 66 | 47.4 | 47.5 | -8.5 | -0.9 | -0.2 | 4.5 |
| 9 | C-NO ₂ | H | H | 3 | E,E,E | | 66.6 | 66.8 | -8.8 | -1.2 | -0.2 | |
| 10 | C-NO ₂ | H | CN | 1 | E | 21 | 25.6 | 29.0 | -6.0 | -4.0 | -0.3 | 5.3 |
| 11 | C-NO ₂ | CH ₃ | CN | 1 | E | 35 | 28.4 | 31.9 | -6.2 | -4.1 | -0.8 | 6.0 |
| 12 | C-2,4-(NO ₂) ₂ | H | H | 1 | E | 23 | 40.0 | 44.8 | -5.9 | -5.9 | -0.4 | 4.9 |

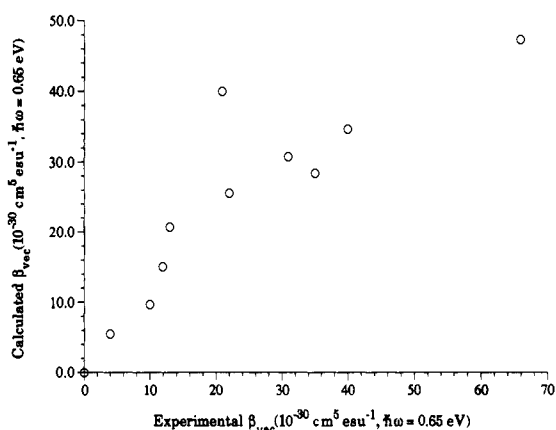
^a Also included is the calculated dipole moment in the x, y, and z directions as defined above. All NLO data are in units of 10^{-30} cm⁵ esu⁻¹; all dipole moment data are in units of debyes. Negative dipole moments indicate negative charge buildup in the positive coordinate direction. ^b Dipole moment and NLO data for molecules 2-8 are from ref 8 and for 10-12 from reference 7.

**Figure 4.** Ferrocenyl chromophores examined in this study along with molecular identification scheme.

analyzing the charge-transfer states contributing to two-level terms of the quadratic hyperpolarizability, even though the $\beta_{\text{vec},3}$ contributions are non-negligible. The insight gained through the predictive ability of the ZINDO model in concert with this empirical assumption provide the best evidence for its application.

Ferrocenyl Derivatives. The electronically asymmetric ferrocenyl chromophores possess the largest microscopic and macroscopic second-order optical nonlinearities reported to date for organometallic architectures. Results from ZINDO-SOS NLO response computations on twelve ferrocenyl derivatives (1-12, Figure 4) are summarized in Table I.³¹ It can be seen that there

(31) The second-order nonlinear optical responses in this contribution differ slightly from those reported in our preliminary communication.^{14b} The variances are due to slight metrical improvements in the idealized structures, as explained in a recent contribution.¹⁶ The most notable geometrical modification is in the polyene bridge portion of extended π -architectures. Specifically, the alternating single-double-single bond distances in the bridging region were set at 1.44-1.36-1.44 Å, rather than assuming all C-C distances to be 1.40 Å. This alteration has the effect of reducing the calculated β_{vec} value by 10-40%, depending upon the specific chromophore.

**Figure 5.** Plot of ferrocenyl chromophore β_{vec} values computed by the ZINDO-SOS procedure versus experimental data from refs 7 and 8. The one anomalous ferrocenyl point ($\beta_{\text{vec}}^{\text{expt}} = 23 \times 10^{-30}$ cm⁵ esu⁻¹; $\beta_{\text{vec}}^{\text{calc}} = 40 \times 10^{-30}$ cm⁵ esu⁻¹) is thought to arise from nonplanarity in the stilbene portion of chromophore 12.

is rather good agreement between calculated and experimental^{7,8} β_{vec} values. The correlation between theory and experiment is illustrated graphically in Figure 5. Note that the quadratic hyperpolarizability ranges from 0.10 to 500×10^{-30} cm⁵ esu⁻¹ for the incident radiation used in these experiments (1.91 μm).^{29,32} However, even with the 10-20% uncertainty usually associated with EFISH measurements,⁷ the ZINDO-SOS derived tensors are in favorable agreement with experiment. Moreover, if we superimpose the previously discussed β_{vec} correlation plot for 25 π -electron organic chromophores¹⁶ onto Figure 5, we see that the ferrocenyl chromophore results fall on the correlation line (Figure 6).

An important electronic structural conclusion from the ZINDO-derived NLO efficiency results is that the inherent quadratic hyperpolarizability (β_{tot}) is essentially equal to the computed NLO response along the ground-state dipole moment direction (β_{vec}). An explanation for this observation can be gained by examining

(32) (a) Cheng, L.-T.; Tam, W.; Stevenson, S. H.; Meredith, G. R.; Rikken, G.; Marder, S. R. *J. Phys. Chem.* **1991**, *95*, 10631-10643. (b) Cheng, L.-T.; Tam, W.; Marder, S. R.; Stiegman, A. E.; Rikken, G.; Spangler, C. W. *J. Phys. Chem.* **1991**, *95*, 10643-10652.

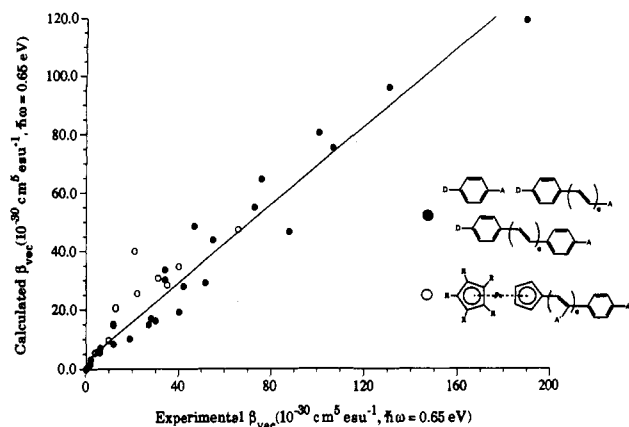


Figure 6. Plot of ZINDO-derived β_{vcc} values for 25 π -electron organic chromophores versus experimental¹⁶ overlaid onto Figure 5. The solid line represents a least-squares fit to the data points. Note that the slope of the line is somewhat less than unity. We attribute this largely to stabilization of the excited state in the solvation medium in which the experiments were performed. Such stabilization will decrease the energy denominators of eqs 2 and 10, thus leading to the increase of β_{obs} compared to β_{calc} .

the Cartesian components (μ_x , μ_y , μ_z) of the computed dipole moment vector. Specifically, the magnitude of the dipole moment in the z direction (i.e., along the cyclopentadienyl-iron-cyclopentadienyl axis) is very small for most chromophores of this class (~ -0.3 D) and only slightly larger for chromophores containing permethylated Cp rings. However, the vast majority of the ground-state dipole moment is located in the stilbene charge-transfer plane (x and y directions). Thus, it is not surprising that $\beta_{\text{tot}} \sim \beta_{\text{vcc}}(\mu\beta)$ in these structures. Placing acceptor substituents perpendicular to the primary charge-transfer direction (10, 11, 12) causes β_{vcc} to deviate slightly from β_{tot} , yet even in these structures, over 90% of the intrinsic nonlinearity will be sampled by EFISH. The ZINDO-derived NLO data clearly show that an EFISH measurement will detect the bulk of the second-order nonlinear optical response for this class of ferrocenyl chromophores.

The one anomalous molecule in the ZINDO-SOS ferrocenyl data is the 2,4-dinitro derivative (12). For this particular molecule, the calculated response ($40.0 \times 10^{-30} \text{ cm}^5 \text{ esu}^{-1}$) is nearly twice the experimental value ($21 \times 10^{-30} \text{ cm}^5 \text{ esu}^{-1}$). However, when these results are compared with the response for the 4-nitro-substituted species (3), ($30.8 \times 10^{-30} \text{ cm}^5 \text{ esu}^{-1}$ calculated versus $34 \times 10^{-30} \text{ cm}^5 \text{ esu}^{-1}$ found by EFISH), it seems likely that a geometrical distortion occurs in 12. A priori, an additional nitro group in an ortho position should increase β_{vcc} , since it aids in stabilizing the predominant charge-transfer excited state of this molecule, thereby lowering the transition energy. The theoretical calculations are in agreement with chemical intuition; however, the EFISH-determined response actually decreases when the second nitro group is added. The only reported crystal structure which relates to this issue is that of *trans*-2,2',4,4',6,6'-hexanitrostilbene, where both of the trinitro-substituted aromatic rings are rotated 60° out of ethylenic plane.³³ We believe a 60° distortion is far too great for 12. In order to qualitatively assess the potential for a geometrical distortion in 12, an MNDO molecular mechanics study^{34,35} was undertaken. In this study, the $\text{FeC}_{10}\text{H}_9$ moiety was replaced by a *p*-methoxyphenyl ($\text{CH}_3\text{O}-\text{C}_6\text{H}_4$) group. The results of this computation suggest that ethylenic H-ortho NO_2 repulsions force the phenyl ring to rotate out of the chromophore plane by 10 – 20° . Such a distortion should

inhibit the degree of π -conjugation in the chromophore, thereby lowering the computed second-order response. A ZINDO-SOS calculation on 12 with the acceptor phenyl group rotated 20° out of the molecular plane yields a β_{vcc} value ($24.3 \times 10^{-30} \text{ cm}^5 \text{ esu}^{-1}$) in quantitative agreement with the EFISH measurement. In the absence of definitive solution-phase evidence for such a structural perturbation, we have chosen to report only the response for the idealized planar structure in Table I along with a caveat regarding possible structural distortions.

It is readily apparent from the ZINDO-SOS results that traditional qualitative arguments for enhancing second-order nonlinear optical responses in organic molecules are completely applicable to the present ferrocenyl chromophores. For instance, the greater the electronic asymmetry between donor (ferrocenyl) and acceptor (A) groups,³⁶ the larger the measured and calculated β responses. As the strength of electronic donor is increased by permethylating the cyclopentadienyl ring, an increase in both computed and observed optical nonlinearity occurs. This is illustrated by comparing a ferrocenyl derivative (3, $30.8 \times 10^{-30} \text{ cm}^5 \text{ esu}^{-1}$) with the corresponding permethylated analogue (4, $34.7 \times 10^{-30} \text{ cm}^5 \text{ esu}^{-1}$). Also, the susceptibilities of ferrocenyl derivatives are largest for molecules containing the strongest electronic acceptors, nitro (3) > aldehyde (7) \approx cyano (6).³⁶ The structure possessing the strongest electronic acceptor in this study, the cationic methylpyridinium derivative (1—largest organometallic $\chi^{(2)}$ to date),⁵ is calculated to possess the largest β response in the ferrocenyl class. However, the inherent charge on this species has prohibited a solution-phase EFISH determination of the microscopic response. While one must be very cautious about inferring microscopic susceptibilities from macroscopic measurements, it is interesting to note that the ratio of $\chi^{(2)}$ values for the two noteworthy ferrocenyl structures ($220 \times \text{urea (1)}:62 \times \text{urea (2)}$)^{5,6} is virtually identical to the ratio of computed molecular β values of $67.6 \times 10^{-30} \text{ cm}^5 \text{ esu}^{-1}$ (1): $21.0 \times 10^{-30} \text{ cm}^5 \text{ esu}^{-1}$ (2). A qualitative analysis of the respective crystal structural data reveals that the packing in both acentric crystal structures is, in fact, very similar.^{5,6}

Also in accord with traditional organic chromophore design guidelines, greater electron delocalization in the ferrocenyl structures leads to enhanced second-order NLO responses. For example, as the number of connecting ethylenic units in the organic ligand is increased from 1 (3) to 2 (8) to 3 (9), the calculated response increases rather dramatically from $30.8 \times 10^{-30} \text{ cm}^5 \text{ esu}^{-1}$ to $47.4 \times 10^{-30} \text{ cm}^5 \text{ esu}^{-1}$ to $66.6 \times 10^{-30} \text{ cm}^5 \text{ esu}^{-1}$. Chromophore 9 was included in this study for comparative purposes even though no experimental data currently exist for this molecule. Finally, the calculated response for the prototypical *cis*-stilbene structure (2, $20.7 \times 10^{-30} \text{ cm}^5 \text{ esu}^{-1}$) is somewhat lower than that for the analogous *trans* derivative (3, $30.8 \times 10^{-30} \text{ cm}^5 \text{ esu}^{-1}$), in accord with conventional chromophore design wisdom.^{2,7} It is interesting to note that the macroscopic response of the *cis* derivative is the second largest in this class, yet the microscopic response is one of the smallest. This dramatically illustrates the effect subtle geometrical differences in molecular structure can have on the crystal-packing architecture and, indirectly, on the NLO response of molecular crystals. Of course, this is not a central issue in self-assembled structures or poled polymeric systems. In summary, the ZINDO-derived quadratic hyperpolarizabilities confirm, in a quantitative fashion, that the ferrocenyl derivatives follow qualitative design rules that have evolved for π -electron organic chromophores.

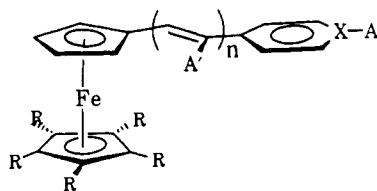
While it is obviously important to reproduce with reasonable accuracy the experimental β_{vcc} responses for the ferrocenyl chromophores, it is equally important to understand, in detail, the electronic origins of the second-order susceptibilities. Let us first discuss the properties associated with the ferrocenyl fragment. This group is usually considered to be an electron-donating substituent when linked to organic fragments,^{37a} and the formation

(33) Gerard, P. F.; Hardy, A. *Acta Crystallogr., Sect. C* **1988**, *44*, 1283–1287.

(34) Dewar, M. J. S.; Zoebisch, E. G.; Healy, E. F.; Stewart, J. J. P. *J. Am. Chem. Soc.* **1985**, *107*, 3902–3909.

(35) The MNDO molecular mechanics study was performed on the CRAY-XMP supercomputer at the Pittsburgh Supercomputer Center. Default parameters were used when optimizing bonds, angles, and dihedral angles in 12.

(36) (a) Swain, C. G.; Lupton, E. C. *J. Am. Chem. Soc.* **1968**, *90*, 4328–4337. (b) Hansch, C.; Leo, A.; Taft, R. W. *Chem. Rev.* **1991**, *91*, 165–195.

Table II. Comparison of Experimental and ZINDO-Derived Optical Absorption Maxima (λ_{max}) and Associated Oscillator Strengths (f) for Various Ferrocenyl Derivatives^a

| | X-A | R | A' | n | isomer | first transition | | | second transition(s) | | |
|----|---------------------------------------|-----------------|----|---|--------|----------------------------|-------------------------|-------------------|----------------------------|-------------------------|-------------------|
| | | | | | | $\lambda^{\text{expt } b}$ | λ^{calc} | f^{calc} | $\lambda^{\text{expt } b}$ | λ^{calc} | f^{calc} |
| 1 | N-CH ₃ ⁺ | H | H | 1 | E | 550 | 521 | 0.04 | 380 | 398 | 0.51 |
| 2 | C-NO ₂ | H | H | 1 | Z | 480 | 363 | 0.04 | 325 | 350 | 0.60 |
| 3 | C-NO ₂ | H | H | 1 | E | 496 | 381 | 0.01 | 356 | 354 | 0.90 |
| 4 | C-NO ₂ | CH ₃ | H | 1 | E | 533 | 468 | 0.01 | 366 | 357 | 0.76 |
| 5 | C-CN | H | H | 1 | Z | 460 | 386 | 0.01 | 308 | 311 | 0.56 |
| 6 | C-CN | H | H | 1 | E | 466 | 392 | 0.01 | 324 | 317 | 0.96 |
| 7 | C-CHO | H | H | 1 | E | 474 | 392 | 0.01 | 338 | 324 | 1.07 |
| 8 | C-NO ₂ | H | H | 2 | E,E | 500 | 510 | 0.01 | 382 | 377 | 1.26 |
| 9 | C-NO ₂ | H | H | 3 | E,E,E | | 458 | 0.01 | | 395 | 1.60 |
| 10 | C-NO ₂ | H | CN | 1 | E | 526 | 473 | 0.01 | 348 | 359 | 0.89 |
| 11 | C-NO ₂ | CH ₃ | CN | 1 | E | 560 | 460 | 0.02 | 366 | 363 | 0.70 |
| 12 | C-2,4-(NO ₂) ₂ | H | H | 1 | E | 536 | 455 | 0.07 | 366 | 355 | 0.46 |
| | | | | | | | | | 413 | 0.31 | |

^aAll energy data are in units of nanometers. ^bSpectroscopic data (in dioxane) for 2-8 are from ref 8, 10-12, from ref 7, and 9, from ref 40.

of a cation (FeCp₂⁺) is a ubiquitous part of ferrocene chemistry.³⁷ Thus, at an initial qualitative level, the relatively large nonlinear optical responses of the ferrocene-derived chromophores are anticipated; they are reminiscent of traditional organic π -chromophoric units, in that a ferrocenyl donor is linked through a π -conjugated network to a nitro acceptor. The reversible oxidation of ferrocene has been shown to involve depletion of a metal-based HOMO.^{37,38} Therefore, it is reasonable to anticipate that the optical "donor" in the ferrocenyl chromophore is the relatively nonbonding pair of predominantly iron-localized oxidatively accessible HOMO electrons.

Two recent investigations have discussed ferrocenyl NLO chromophores in a quantum chemical context. Marder, Cheng, et al. have attempted to extract linear and nonlinear optical information from an extended-Hückel ground-state calculation on 3;^{7,8} such one-electron models generally do not provide quantitative accuracy. In addition, a recent finite-field study by Waite and Papadopoulos³⁹ examined the α and γ properties of ferrocenyl derivatives; calculations using this formalism do not provide frequency-dependent response information. Since the ZINDO-SOS responses discussed in the present study are derived from a reasonable semiempirical model with a consistent treatment of both ground and excited states, our procedure allows connections to be made between microscopic responses and molecular architecture/electronic structure. That is, we can pinpoint those features that lead to large or small responses in a particular class of chromophoric structures within a molecular orbital context.

Scheme I enumerates the physically reasonable assumptions necessary to understand the electronic origins of the NLO response for the prototypical molecules *trans*-1-ferrocenyl-2-(4-nitrophenyl)ethylene (3), which will serve as a generic model for all ferrocenyl chromophores examined in this work. Note that $\beta_{\text{vec},3}$ for this molecule ($-41.0 \times 10^{-30} \text{ cm}^5 \text{ esu}^{-1}$) is of opposite sign and approximately half the magnitude of $\beta_{\text{vec},2}$ ($71.8 \times 10^{-30} \text{ cm}^5 \text{ esu}^{-1}$), in accord with the common observations previously discussed. In making the assumption that an understanding of the β response can be gained by analyzing all two-level contributions, we have

Scheme I. Analysis of β for Molecule 3

| | |
|---|-------|
| Two-level contribution ($\beta_{\text{vec},2}$) | 71.8 |
| Three-level contribution ($\beta_{\text{vec},3}$) | -41.0 |
| Total ($\hbar\omega = 0.65 \text{ eV}$) | 30.8 |
| β_{vec} in units of $10^{-30} \text{ cm}^5 \text{ esu}^{-1}$ | |

Assumption 1: Three-level terms scale as two-level terms. Therefore, understanding two-level terms will provide qualitative understanding of β .

76% of the total two-level contribution comes from one two-level term involving a MLCT at 354 nm with an oscillator strength of 0.91.

Assumption 2: The two-level contribution is dominated by one excited state. Therefore, understanding this excited state will provide qualitative understanding of β .

$$\Psi_{\text{Excited State}} = 0.50 \Phi_{2a \rightarrow 5a} + 0.77 \Phi_{4a \rightarrow 5a}$$

where 2a and 4a are filled orbitals and 5a is an unfilled orbital.

Assumption 3: The β -determining excited state transition is dominated by two transitions between molecular orbital configurations as dictated by the ZINDO CI coefficients. A description of these transitions will lead to a chemical interpretation of β .

reduced the nonlinear optical problem to an extension of the linear optical problem. That is, if a satisfactory description of the predominant electronic transitions can be obtained, a chemically oriented, molecular description of the second-order response will immediately follow. It is encouraging to note that the ZINDO algorithm has been shown to reproduce reliably the experimental features of ferrocene MLCT transitions.^{22b}

In Table II, we tabulate the experimental and calculated details of the optical absorption spectra of the ferrocenyl chromophores 1-12. The theoretical and experimental data^{7,8} for these molecules show two optical transitions, with the exception of the 2,4-dinitro species (12), where the calculated spectrum contains three transitions while only two are found experimentally. Note that the ZINDO-derived lowest energy "transitions" for all structures possess very small oscillator strengths (0.01-0.04) relative to those of the higher energy transitions (0.46-1.60). When the computed optical properties are compared with those from experiment, it can be seen that the ZINDO method reliably predicts the intense shorter wavelength transitions. However, it less accurately predicts the characteristics of the weak longer wavelength optical absorptions. For example, the ZINDO-derived optical transitions

(37) See, for example: (a) Nesmeyanov, A. N.; Perevalova, E. G.; Gubin, S. P.; Grandberg, K. I.; Kozlovsky, A. G. *Tetrahedron Lett.* **1966**, 22, 2381-2387. (b) Perevalova, E. G.; Reshetova, M. D.; Grandberg, K. I. *Methods of Organometallic Chemistry: Organoiron Compounds; Ferrocene*; Nauka: Moscow, USSR, 1983. (c) *Gmelin Handbook of Inorganic Chemistry: Fe-Organoiron Compounds*, 8th ed.; Springer-Verlag: Berlin, 1986; Pt. A8, Ferrocene.

(38) See, for example: Gubin, S. P. *Pure Appl. Chem.* **1970**, 23, 463-487.

(39) Waite, J.; Papadopoulos, M. G. *J. Phys. Chem.* **1991**, 95, 5426-5431.


of the pyridinium ferrocenyl derivative (**1**) are at 398 nm ($f = 0.71$) and 521 nm ($f = 0.04$), while the observed absorptions occur at 380 nm ($f = 0.8$) and at 550 nm ($f = 0.2$).⁴⁰⁻⁴² The ZINDO treatment clearly underestimates the strength of the low-energy linear transitions, even though the computed nonlinear optical properties are in agreement with experiment. As we will show, the reason for this is that the higher energy features are MLCT in nature and are responsible for the nonlinear response of these derivatives, while the lower energy excitations are ligand-field transitions, which are essentially irrelevant to the NLO response.

To gain insight into the linear optical properties of ferrocenyl derivatives, we first analyze the absorption spectrum of ferrocene. The dominant spectral feature is a broad band near 220 nm.⁴³ Several significantly weaker transitions lie at lower energies, the most commonly quoted being at 440 nm.⁴³ Both theoretical^{22b,44} and experimental^{43,45} studies have shown that the 440-nm transition is a ligand-field "d-d" excitation. The exact assignment of the highly allowed 220-nm transition remains controversial; however, theory and experiment agree that it is either LMCT or MLCT in origin (probably MLCT).^{22b,43-46}

Toma and co-workers have investigated the substituent dependence of the ferrocenyl ligand-field transition.^{47,48} This band is found to be very sensitive to electron-withdrawing substituents in arylferrocene derivatives⁴⁷ and very dependent upon the electron acceptor in 1-aryl-2-ferrocenylethylenes⁴⁸ such as those examined in this contribution. Moreover, the magnitude of the bathochromic shift in these structures correlates well with the Hammett σ^+ parameter of the electron acceptor group.⁴⁸ The transition with the 440-nm parentage can significantly red-shift when acceptor strength or delocalization length is increased.⁴⁶ For example, a 471-nm transition ($\epsilon = 1310 \text{ M}^{-1} \text{ cm}^{-1}$ in isoctane) is observed in $\text{CpFeC}_5\text{H}_4\text{-NO}_2$, and a 520-nm optical absorption ($\epsilon = 5200 \text{ M}^{-1} \text{ cm}^{-1}$ in isoctane) is found in the optical spectrum of $\text{CpFeC}_5\text{H}_4\text{-N=N-C}_5\text{H}_4\text{FeCp}$. These "d-d" transitions are highly allowed relative to typical ligand-field transitions and are energetically located in the vicinity of the λ_{max} measured for the ferrocenyl chromophores. Toma and co-workers have also found these so-called ligand-field transitions to have very large ϵ values ($>5,000 \text{ M}^{-1} \text{ cm}^{-1}$) in some cases.⁴⁸

From the above discussion, it is not difficult to extrapolate to the electronic situation in **1**, where the observed 550-nm transition is likely a ligand-field transition with some admixed cyclopentadienyl character. It is not unrealistic to assume that the ligands with large σ^+ coefficients found in chromophores **1-12** could red-shift the 440-nm ligand-field ferrocene absorption far into the visible. In addition, Laporte-forbidden ligand-field transitions can "steal" intensity from highly allowed charge-transfer transitions via coupling through appropriate vibrational modes.⁴⁹ The magnitude of the coupling matrix elements will be particularly large for structures possessing MLCT or LMCT excitations in the energetic proximity of the ligand-field transi-

Table III. Comparison of ZINDO-Derived β_{vec} Values for Ferrocenyl Derivatives and their Methoxyphenyl Analogues^a



| A' | n | isomer | β_{vec} | |
|----|---|-----------------------|---|--|
| | | | X = $\text{FeCp}(\text{C}_5\text{H}_4)$ | X = $\text{CH}_3\text{OC}_6\text{H}_4$ |
| H | 1 | Z | 20.7 (2) | 19.8 |
| H | 1 | E | 30.8 (3) | 34.2 |
| H | 2 | E,E | 47.4 (8) | 50.5 |
| H | 3 | E,E,E | 66.6 (9) | 68.0 |
| CN | 1 | E | 25.6 (10) | 26.8 |
| H | 1 | (2,4-dinitro species) | 40.0 (12) | 42.7 |

^a All NLO data are at $\hbar\omega = 0.65 \text{ eV}$ in units of $10^{-30} \text{ cm}^5 \text{ esu}^{-1}$.

tions.⁵⁰ The charge-transfer excitations in transition-metal molecules possessing significant metal-ligand covalency tend to display optical characteristics arising from the large effective coupling matrix elements.⁴⁹ Thus, the highly covalent nature of the metal-ligand bonding is expected to increase the (formally forbidden) oscillator strengths of d-d transitions in the ferrocenyl structures far beyond what is observed in classical coordination complexes.⁴⁹ Note that the Herzberg-Teller expansion of the full Hamiltonian that accomplishes the vibrational coupling is omitted in the present work. Therefore, it is not surprising that the present computational procedure does not reproduce the characteristics of the predominantly d-d transitions.

There is thus compelling experimental and theoretical evidence that the low-energy transitions in **1-12** can be assigned as ligand-field-based. As such, they should contribute little to the NLO response. In addition to having modest f values, the small solvatochromic shift measured for these optical excitations relative to those for the allowed MLCT bands is indicative of a small $\Delta\mu_{\text{gr}}$.⁴⁰ Our computations indicate that the weak ligand-field transition in the ferrocenyl prototype (**3**) can be described by a charge-transfer of 0.78 t_{2g} -like electrons into 0.64 e_g -like electrons and 0.14 cyclopentadienyl electrons. In essence, this represents a complete charge transfer from a metal-localized state of pseudo- t_{2g} symmetry into a metal-localized state of pseudo- e_g symmetry, resulting in a very small $\Delta\mu$. Therefore, while the d-d transition energies may be attractive for chromophore design, the small $\Delta\mu$ and modest f values associated with these transitions argue against exploiting them in NLO chromophoric materials. In a simple two-level picture (eq 10), they are predicted to afford small values of β .

We now turn to the shorter wavelength transitions in the ferrocenyl chromophores. If an MLCT assignment is correct, such excitations should dominate the second-order nonlinear optical response in chromophores **1-12**. The λ of this particular excitation can be traced back to the 243-nm transition in the parent ferrocene as shown by Bozak.⁴⁶ Note that most of the ZINDO-derived λ values for the higher energy transitions are within 15 nm of the observed absorption energy, as shown in Table II. The prototypical chromophore **3** illustrates the good agreement between theory and experiment for this transition (experiment = 356 nm, theory = 354 nm).⁵¹ The excellent agreement between theory and experiment for both the higher energy linear optical transition and the second-order quadratic hyperpolarizability strongly suggests that the lower energy ligand field-based optical transitions are essentially NLO inactive and that the intense MLCT bands dictate the NLO response in these structures. Interestingly, recent degenerate four-wave mixing experiments⁵² suggest that only the higher energy transitions contribute significantly to the observed

(40) Marder, S. R.; Perry, J. W.; Schaefer, W. P.; Tiemann, B. G. *Organometallics* **1991**, *10*, 1896-1901.

(41) The oscillator strengths were estimated from the published optical spectrum for **1**⁴⁰ using the formula $f_{\text{ge}} \approx 4.319 \times 10^{-9} (\epsilon_{\text{max}})(\Delta\nu)^{1/2}$.⁴² Since we do not have actual optical spectra for the other chromophores discussed in this work, it is impossible to convert between molar absorptivity and oscillator strength due to the $\Delta\nu$ quantity.

(42) Suzuki, H. *Electronic Absorption Spectra and Geometry of Organic Molecules*; Academic Press: New York, 1967; p 9.

(43) (a) Scott, D. R.; Becker, R. S. *J. Chem. Phys.* **1962**, *35*, 516-531. (b) Armstrong, A. T.; Smith, F.; Elder, E.; McGlynn, S. P. *J. Chem. Phys.* **1967**, *46*, 4321-4328. (c) Sohn, Y. S.; Hendrickson, D. C.; Gray, H. B. *J. Am. Chem. Soc.* **1971**, *93*, 3603-3612.

(44) (a) Rohmer, M. M.; Veillard, A.; Wood, M. H. *Chem. Phys. Lett.* **1974**, *29*, 466-468. (b) Rösch, N.; Johnson, K. H. *Chem. Phys. Lett.* **1974**, *24*, 179-183.

(45) (a) Tarr, A. M.; Wiles, D. M. *Can. J. Chem.* **1968**, *46*, 2725-2731. (b) Černý, V.; Pavlík, I.; Kustková-Maxová, E. *Collect. Czech. Chem. Commun.* **1976**, *41*, 3232-3244.

(46) Bozak, R. E. *Adv. Photochem.* **1972**, *8*, 227-244.

(47) Toma, Š.; Gáplovský, A.; Hudeček, M.; Langfelderová, Z. *Monatsh. Chem.* **1985**, *116*, 357-364.

(48) Toma, Š.; Gáplovský, A.; Elečko, P. *Chem. Pap.* **1985**, *39*, 115-124.

(49) (a) Reference 3a, Chapters 4 and 6. (b) Reference 3b, Chapter 1.

(50) Fenske, R. F. *J. Am. Chem. Soc.* **1967**, *89*, 252-256.

(51) As one would anticipate from the distortion arguments presented earlier in this contribution, the computed absorption characteristics of the 2,4-dinitro derivative (**12**) are not in agreement with experiment and are an exception to the excellent correlation between theory and experiment.

(52) Ghosal, S.; Samoc, M.; Prasad, P. N.; Tufariello, J. J. *J. Phys. Chem.* **1990**, *94*, 2847-2851.

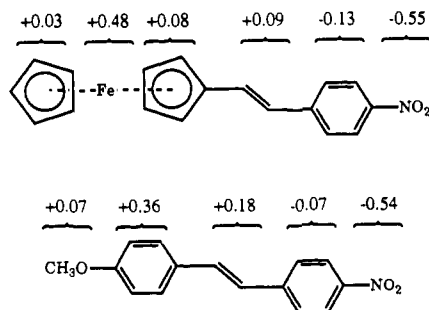
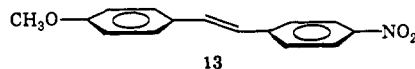


Figure 7. The difference in electronic populations between ground state and crucial excited state for a prototypical ferrocenyl derivative and a traditional organic chromophore as determined by ZINDO calculations. A negative population is indicative of an increase in electron density in the charge-transfer process.

third-order responses in representative ferrocenyl chromophores. Specifically, the low-lying resonances (labeled as d-d) do not appear to make an important contribution to the third-order response in these molecules, while the higher lying resonances (labeled as π - π^*) appear to dominate the third-order susceptibility.⁵²

If in fact, one excited state is primarily responsible for the observed second-order susceptibility, the ferrocene derivatives should bear strong resemblances to classic two-level systems, such as the push-pull polyenes. As pointed out by Marder and Cheng,⁸ the experimental NLO response of **3** is essentially identical to that of the corresponding methoxyphenyl analogue **13**.



In order to examine the relationship between classic organic chromophores and the ferrocenyl chromophores in more detail, we replaced the ferrocenyl group in selected chromophores with a methoxyphenyl ($\text{CH}_3\text{O}-\text{C}_6\text{H}_5$) moiety. From the results of this numerical study (Table III), it is immediately obvious that this structural variation leaves the computed second-order response essentially unchanged. For example, the β_{vec} ratio of the organic to ferrocenyl analogue is 19.8/20.7 for **2**, 50.5/47.4 for **8**, and 42.7/40.0 for the anomalous dinitro derivative **12**. This similarity strongly suggests that there is common electronic origin of the nonlinear optical response in these two classes of chromophores and that the predominantly metal-centered d-d excitations are unimportant in determining the NLO response.

To further probe the connection between the ferrocenyl structures and their organic counterparts, the one charge-transfer state that dominates the NLO response in **3** and **13** will be analyzed. The calculated changes in charge between ground and excited state are shown in Figure 7. In each chromophore, the nitro acceptor group receives ~ 0.55 electrons in the charge-transfer process. The ferrocene donor supplies 0.59 electrons to the π -network in the charge-transfer excitation in **3**, with most of this charge density originating at the iron center. In **13**, the methoxyphenyl moiety contributes 0.43 electrons to the charge transfer, with most of the electron density derived from the phenyl group appended to the methoxy substituent rather than from the methoxy moiety itself. We have found this to be true for all push-pull stilbenes examined to date. That is, the phenyl group adjacent to the electron-donating moiety, rather than the donor group itself serves as the effective donor in the charge-transfer transition. In contrast, the NO_2 electron acceptor serves as the predominant electron sink in the charge-transfer transition. Overall, the change in regional electron populations associated with the dominant charge-transfer optical transition in **3** are virtually identical to those computed for **13**, providing additional evidence for the strong NLO similarity between the ferrocenyl chromophores and their methoxyphenyl counterparts.

The ZINDO-SOS algorithm permits decomposition of the state-to-state transitions dictating the NLO response into transitions between molecular configurations (i.e., transitions between

Scheme II. Analysis of β for Molecule 13

| | |
|---|-------|
| Two-level contribution ($\beta_{\text{vec},2}$) | 84.4 |
| Three-level contribution ($\beta_{\text{vec},3}$) | -50.2 |
| Total ($\hbar\omega = 0.65$ eV) | 34.2 |
| β_{vec} in units of 10^{-30} cm ³ esu ⁻¹ | |

Assumption 1: Three-level terms scale as two-level terms. Therefore, understanding two-level terms will provide qualitative understanding of β .

86% of the total two-level contribution comes from one two-level term involving a transition at 353 nm with an oscillator strength of 1.17.

Assumption 2: The two-level contribution is dominated by one excited state. Therefore, understanding this excited state will provide qualitative understanding of β .

$$\Psi_{\text{Excited State}} = 0.91 \Phi_{4a} \rightarrow 5a$$

where 4a is a filled orbital and 5a is an unfilled orbital.

Assumption 3: The β -determining excited state transition is dominated by one transition between molecular orbital configurations as dictated by the ZINDO CI coefficients. A description of this transition will lead to a chemical interpretation of β .

filled and unfilled molecular orbitals). For **13**, the predominant excited state involves little CI mixing between configurations and is found to be primarily a HOMO to LUMO transition (Scheme II). The data in Scheme I suggest that the important state in **3** involves significant CI mixing between two configuration transitions, one of them also a HOMO-LUMO excitation. By decomposing the computed response into configurational excitations and describing these excitations in molecular orbital terms, a chemically-oriented rationalization of the NLO response will emerge.

Simplified molecular orbital diagrams depicting frontier orbital interactions in **3** and **13** are displayed in Figures 8 and 9, respectively. Note that all σ interactions have been deleted from these pictures, since they have little effect on the nonlinear optical responses. Since the molecular point group of **3** and **13** is C_1 , all molecular orbitals are of "a" symmetry and can mix in both the SCF and CI portions of the computation. We have chosen to divide the two chromophores into a common *p*-nitrovinylbenzene fragment combining with a ferrocenyl fragment in **3** and a methoxyphenyl fragment in **13**. The common nitro-containing fragment possesses a HOMO that is primarily of ethylenic bonding character and a LUMO of appreciably higher energy that is nitro-centered.

The electronic details of the ferrocenyl fragment in **3** are straightforwardly related to the well-studied electronic structure of ferrocene.⁵³ The three lower lying metal orbitals in ferrocene (d_{xy} , $d_{x^2-y^2}$, and d_{z^2}) are essentially the pseudo- t_{2g} set of d_π orbitals and are fully occupied in a d^6 Fe(II) system.⁵³ While there is disagreement⁵⁴ over the exact ordering of these three orbitals in the parent ferrocene molecule, their relative positions are not crucial for our discussion. Also note the presence of two unoccupied metal orbitals at significantly higher energy. These are the metal-ligand antibonding e_g set commonly associated with octahedral structures. When the ferrocenyl fragment interacts with the styrenyl moiety, only one of the filled d_π orbitals will be significantly perturbed by the interaction; the other two d_π orbitals are virtually unaffected due to limited overlap (spatial constraints) with the π -fragment. In-phase and out-of-phase linear combinations of the two interacting fragment orbitals produce molecular orbitals **2a** and **4a** (Figure 10), with the latter being the molecular

(53) (a) The actual symmetry notation that we use for orbitals varies. For clarity, the crystal field notations e_g and t_{2g} are useful for discussing metal d-levels. In actual MO calculations, it is more appropriate and meaningful to use the proper point group symmetry (a_1 , e_1) labels. (b) Lauher, J. W.; Hoffmann, R. *J. Am. Chem. Soc.* 1976, 98, 1729-1742 and references therein.

(54) Cowley, A. H. *Prog. Inorg. Chem.* 1979, 26, 46-160.

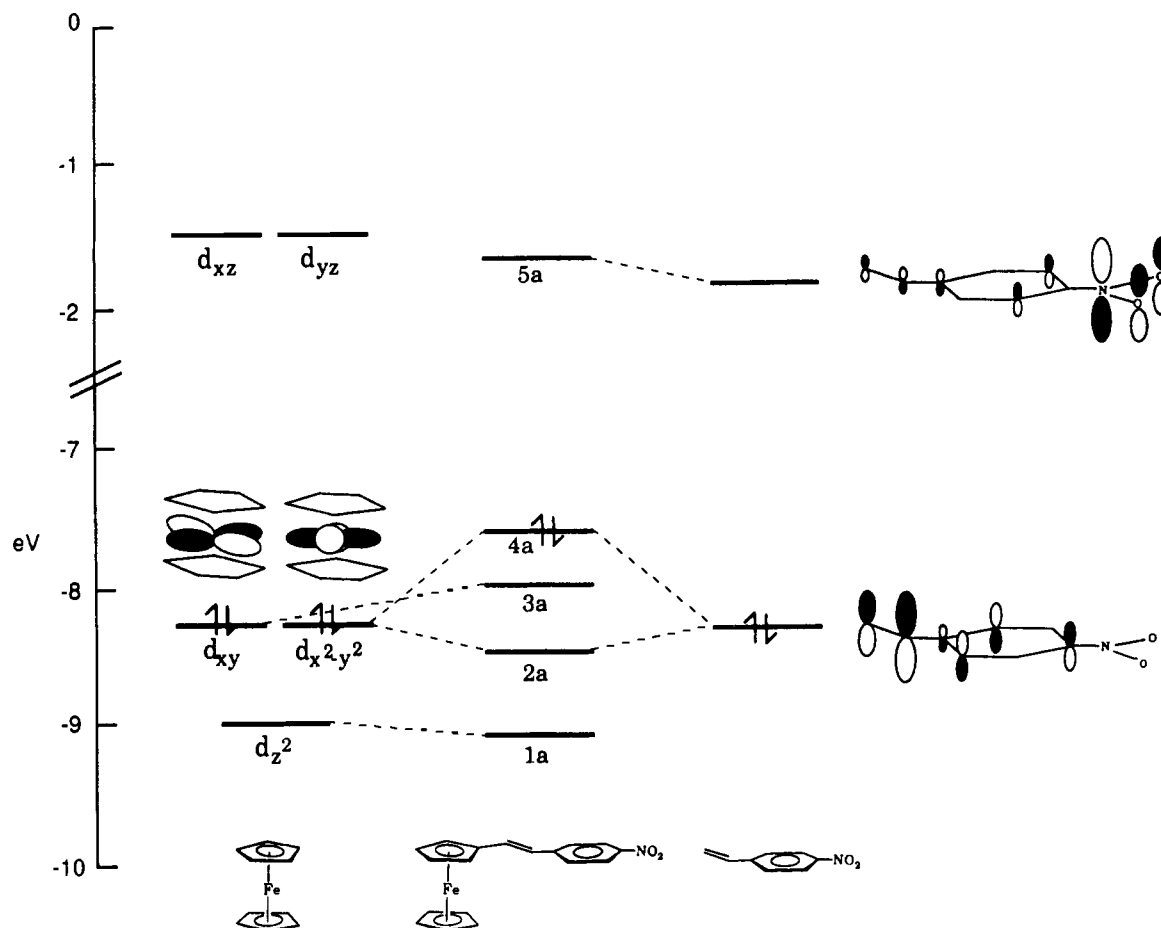


Figure 8. Molecular orbital diagram for the representative ferrocenyl chromophore 3.

HOMO. As detailed in Scheme I, it is precisely these two molecular orbitals that are involved in the "NLO-active" state-to-state charge-transfer transition in 3. Specifically, 50% of the dominant optical excitation in 3 is 4a-to-LUMO in character, 25% is 2a-to-LUMO, and the remainder is derived from a host of other configuration space excitations. From Figure 8 it is clear that orbitals 2a and 4a contain significant contributions from both interacting fragments. This covalent mixing reflects the energetic similarity of the respective orbitals. The result of configuration interaction for these two configuration space transitions is to constructively add the ferrocenyl (principally $d_{x^2-y^2}$) contributions and destructively add the nitro-containing ligand (principally ethylenic) components. In summary, the "donor" state is primarily iron in character with a small fraction of the electron density in the ethylenic region. Over 95% of the iron contribution originates from the $d_{x^2-y^2}$ orbital. The residual metal character (d_{xz}) serves to point the $d_{x^2-y^2}$ function toward the π -electron density in the bridging region of the organic fragment, thereby increasing the overlap between the metal and organic fragments.

The LUMO of the nitro fragment becomes the LUMO (orbital 5a) of 3 as depicted in the interaction diagram (Figure 8). The fragment orbital is essentially unperturbed (both spatially and energetically) upon interaction with the ferrocenyl fragment, since the majority of its electron density is spatially distant from the interaction region. This orbital is primarily centered on the acceptor group, so that modifying the accepting moiety should substantially alter the energy of this fragment orbital and subsequently the molecular LUMO as well. That is, a weaker acceptor moiety, such as a CN or COOCH_3 , will increase the SCF energy of the LUMO.

Before using the orbital picture to rationalize trends observed for the β_{vec} values in 1–12, we first analyze the 4-methoxy-4'-nitrostilbene chromophore (13) within the molecular orbital formalism. The orbitals of the methoxyphenyl fragment (Figure 9) are derived from a bonding and antibonding interaction between

the phenyl ring and the methoxy lone pair. The bonding, lower energy fragment orbital is predominantly methoxy lone pair in character as pictured in Figure 9. This orbital is essentially unperturbed upon interaction with the nitro-containing moiety and results in the 3a molecular orbital. Somewhat surprisingly, the oxygen-based molecular orbital is *not* a major contributor in the charge-transfer excitation that dictates β_{vec} . The second methoxyphenyl orbital, the higher energy of the two fragment functions, is delocalized over the entire phenyl ring and therefore can efficiently interact with the ethylenic-centered HOMO of the nitro-containing fragment. The interaction between these two orbitals produces a stabilized MO (orbital 2a) and a highly destabilized orbital (4a, HOMO). As was the case for 3, the LUMO of the *p*-nitrostyryl fragment is essentially unperturbed by the interaction and becomes the LUMO (orbital 5a) of 13. As shown in Scheme II, the excitation that dominates the second-order nonlinear optical response in 13 is accurately described by a 4a to 5a (HOMO to LUMO) transition. From the pictures of the relevant fragment orbitals in Figure 9, it is clear that the charge transfer will occur from the phenyl ring adjacent to the methoxy group to the nitro moiety. Recall this charge redistribution is exactly what the electron density change results suggested (Figure 7). Again, the orbital picture accurately represents the state-to-state charge-transfer populations. At first glance it may seem surprising that the donor substituent in 13 does not play a more active role in the important charge-transfer transition associated with the large second-order NLO response. However, the donor moiety will indirectly influence the charge transition by raising the SCF orbital energies of the appended phenyl ring.

The similarity of the MO orderings of the prototypical ferrocenyl chromophore and its methoxyphenyl analogue, as shown by Figures 8 and 9, is remarkable. The functional characteristics as well as the energetic values for the key molecular orbitals are virtually identical in 3 and 13. For example, both donor orbitals ($d_{x^2-y^2}$ in 3 and phenyl ring in 13) are nearly of equal energy and

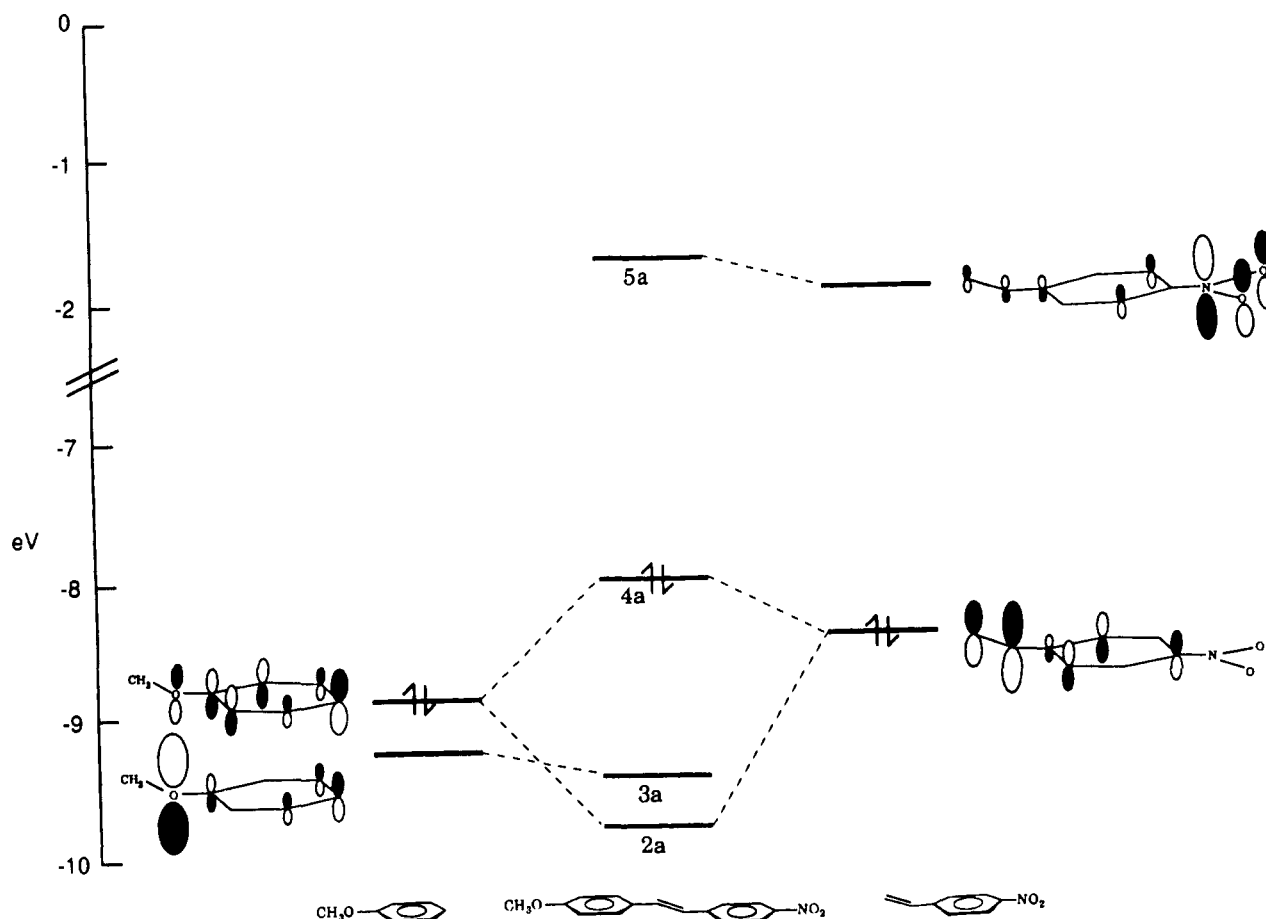


Figure 9. Molecular orbital diagram for the corresponding methoxyphenyl analogue of 3.

covalently interact with ethylenic bridge orbitals of the acceptor. In addition, the acceptor-based LUMOs in the two chromophores are essentially interchangeable. The admixture of $2a \rightarrow 5a$ in the dominant excitation ($4a \rightarrow 5a$) observed in 3 is somewhat larger than that found in 13 as expected from perturbation theory (the $2a \rightarrow 5a$ transition energy is closer to the $4a \rightarrow 5a$ excitation energy in 3 than it is to that in 13) as shown in Schemes I and II. The dominant components of the important charge-transfer transition are similar in 3 and 13, but as Figure 7 shows, the real charge transfer originates mostly from the metal in 3 but from the π -donor in 13. To describe this properly, the simple HOMO \rightarrow LUMO transition appropriate for 13 is admixed (Scheme I) with $2a \rightarrow 5a$ in 3. Since similar charge-transfer patterns dominate the NLO response and chromophores 3 and 13 and their constituent electronic structures are very similar, it is perhaps not surprising that ferrocenyl and methoxyphenyl donor units produce similar NLO responses when introduced into conventional push-pull chromophoric architectures.

One may wonder how traditional chromophore design guidelines are manifested in the MO diagrams of Figure 8 and 9, or more specifically, how experimentalists can use the orbital picture to rationalize NLO responses. As mathematically described in eq 10,²⁸ $\Delta\mu_{gn}$, f_{gn} , and ω_{gn} ($= E_{gn}/\hbar$, $= 2\pi c/\lambda_{gn}$) are the crucial two-level parameters in chromophore design. For the present discussion, the oscillator strength (f) in the Oudar formula will be rewritten as a function of r_{gn}^2 and E_{gn} to yield the simplified, zero-frequency two-level prescription (eq 11). The energy of the

$$\beta \propto \frac{r_{gn}^2 \Delta\mu_{gn}}{E_{gn}^2} \quad (11)$$

dominant excitation (E_{gn} or hc/λ_{gn}) can be monitored by probing the perturbations of the orbital energy levels involved in the charge-transfer transition. For example, permethylation of the cyclopentadienyl ring in the prototype raises the energy of the d_x

donor orbital from 6.99 eV in 3 to 7.13 eV in 4. Since the derivatization should have little effect on the orbital energies of the acceptor levels (verified by our computations), the increase in d orbital energy should produce a bathochromic shift in the MLCT transition if effects due to CI remain approximately constant. As predicted, the principal optical transition in 3 (354 nm) shifts to 357 nm in the permethylated derivative 4. In a similar fashion, altering the acceptor moiety should significantly change the energy of the acceptor unit without affecting the donor. Therefore, decreasing the acceptor strength by replacing the nitro group with a CN (6) or COH (7) group should raise the SCF energy of the LUMO, thereby hypsochromically shifting the charge-transfer transition. As reported in Table II, the experimentally measured MLCT excitation blue-shifts from 354 nm in 3 to 317 nm in 6 and 324 nm in 7. Similarly, increasing the acceptor strength should red-shift the dominant transition as is observed for 1.

Limited qualitative information on the $\Delta\mu$ quantity can also be obtained from the orbital picture. Quantum chemical computations in concert with MO arguments can determine if a particular charge-transfer excitation is effectively one-dimensional or multidimensional. The orbital pictures for 3, for example, indicate that the electronic redistribution associated with the dominant MLCT transition involves only one of the cyclopentadienyl rings. That is, two-dimensional or three-dimensional charge transfer, a situation that will greatly diminish $\Delta\mu$, is not an issue here. Unfortunately, there is no simple relationship between $\Delta\mu$ and fragment energetics, as pointed out in a recent contribution.^{1d} Thus, a more complete description of $\Delta\mu$ within our model will require an atom-by-atom charge analysis such as that provided in Figure 7.

Perhaps the most unique aspect of the ferrocenyl chromophores, in comparison with other organometallic nonlinear optophores, is that they possess low-lying charge-transfer excitations with reasonably large oscillator strengths (>0.50). A rationale for these

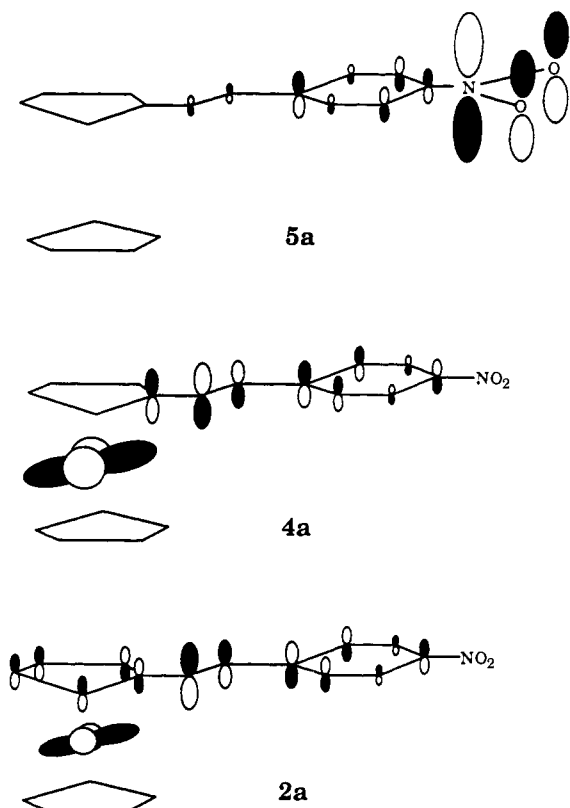


Figure 10. Frontier molecular orbitals of **3** involved in the dominant charge-transfer excitation. The excitation is comprised of a mixture of **2a** \rightarrow **5a** with **4a** \rightarrow **5a**, to yield the population changes in Figure 7. Note that adding **2a** to **4a** gives destructive interference everywhere except on the metal center; this, then, is the source for charge-transfer.

anomalously large oscillator strengths ($\propto r_{gn}^2$) is available through the orbital pictures of Figures 8 and 9. Examining the physical interpretation of r_{gn} (transition moment) between a ground state (represented by a donor molecular orbital) and an excited state (represented by an acceptor molecular orbital) for a traditional π -electron organic chromophore affords a qualitative understanding of the "allowedness" of a given transition. The transition moment (r_{gn}) for the dominant $\pi \rightarrow \pi^*$ excitation in a π -organic chromophore can be written as $e\langle\psi_g|x|\psi_n\rangle$, assuming x is the charge-transfer direction. For push-pull species, such as those of interest here, the dominant transition is from the HOMO (largely centered in the donor region, with some extension onto the ethylenic bridge) to the LUMO (largely acceptor-centered, with some ethylenic bridge extension). The overlap density, and therefore the r_{gn} integral, will vanish unless both HOMO and LUMO have significant extension onto the ethylenic bridge.⁵⁵

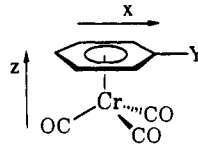
From these rather simplified arguments, it appears that reasonable oscillator strengths in highly asymmetric (large $\Delta\mu$) chromophores will only occur in significantly covalent structures. That is, a non-negligible amount of electron density must be present in the π -backbone bridge of potential chromophores. In the specific case of stilbene-based derivatives, the crucial functions are the p_π functions on the ethylenic carbon atoms. Our prototypical chromophores **3** and **13** meet the large f_{gn} criterion, as can be seen in Figures 8, 9, and 10. The charge-transfer transitions in both structures possess non-negligible electron densities in the intermediate region. If the nitro group is replaced by a weaker acceptor, relatively more electron density should be present in the bridging region, and this may be associated with an increase in the relevant oscillator strength. As reported in Table II, the oscillator strength of **3** ($f = 0.90$) is less than those computed for a cyano ($f = 0.96$) or an aldehyde ($f = 1.07$) substitution. In summary, the more covalent the electronic structure or, more

empirically, the greater the interactions found in the molecular orbital diagram, the greater the electron density in the bridging region and the larger the oscillator strength. The foregoing discussion was included in this contribution because ferrocenyl-based chromophores not only have the largest organometallic β values discovered to date but also possess anomalously large MLCT oscillator strengths compared with most other organometallic molecules.^{3a}

We now contrast our description for electronic origin of the second-order response in ferrocenyl chromophores to that recently proposed in the literature.⁸ On the basis of a qualitative bonding discussion, the authors of the previous contribution suggest that (1) the low-lying excitations (assigned as MLCT transitions) and the higher lying excitations (assigned as ligand-to-ligand charge-transfer excitations) make significant contributions to β_{vec} , (2) poor coupling between the metal center and the cyclopentadienyl ligand lowers the effectiveness of the metal center as a donor, (3) the ferrocenyl donor behaves very much like a methoxyphenyl donor on the basis of experimental evidence, and (4) the metal plays a key role in determining hyperpolarizabilities in these chromophores.

Point 3 is probably the most important in contrasting organic and organometallic NLO chromophores and is in full agreement with our quantitative computations. Perhaps the primary disagreement between our results and those presented in ref 8 is the nature and relative importance of the two optical transitions in the ferrocenyl chromophores. In the previous work, a ground-state one-electron extended-Hückel computation was performed on **3**, and the charge-transfer excitations were *inferred* from the electronic structure results.⁸ In contrast, the present approach allows a full analysis of the electronic origins of β_{vec} by computing the contribution of each linear optical excitation to the second-order response and by linking the spectral features with transitions between filled and unfilled molecular orbitals. From our computations, we find that the higher lying transitions are MLCT and not LLCT as previously proposed. We assert that the lower lying transitions are in fact ligand-field-based excitations of unusually (but not unprecedentedly) large oscillator strengths, in agreement with the assignments of Toma and co-workers,^{47,48} and not MLCT transitions as hypothesized by Marder, Cheng, et al.⁸

Reference 8 also concludes that the two-level model does *not* apply to the ferrocenyl chromophores because both optical transitions make significant contributions to β_{vec} . This assertion can be tested by examining the relationships between experimentally determined linear and NLO properties for specific chromophores. For example, we see from the experimental data⁸ that the low-energy peak for chromophore **4** occurs at 533 nm compared to 500 nm for chromophore **8**. However, the experimental β value of the former is significantly less (**4**, 40×10^{-30} cm⁵ esu⁻¹) than that of the latter (**8**, 66×10^{-30} cm⁵ esu⁻¹). In other words, a significant blue-shift in the low-energy transition is accompanied by a significant *increase* in the quadratic hyperpolarizability, in disagreement with conventional chromophore design phenomenology based upon minimizing the denominator of eq 11. In contrast, the correlation of β to the higher lying absorptions (**4**, 357 nm; **8**, 377 nm) fits nicely within the traditional two-level design guidelines. Additional empirical evidence that the lower lying ferrocenyl excitations do not significantly contribute to β_{vec} comes from comparison with organic chromophores. Conventional organic chromophores containing charge-transfer excitations near 500 nm possess extremely large nonlinear optical responses, on the order of $150\text{--}300 \times 10^{-30}$ cm⁵ esu⁻¹ (for $\hbar\omega = 0.65$ eV).³² However, the NLO responses of the ferrocenyl chromophores are not nearly as large under comparable measurement conditions as would be expected if these low-energy transitions indeed govern the magnitude of the second-order response. Our calculations show that only the higher energy ferrocenyl excitations (MLCT) are necessary to understand the NLO response and that an appropriate two-level model *does apply* to this class of chromophores; the higher energy MLCT excitations dictate β , while the lower frequency ligand-field-based excitations contribute little. Since the "ligand-field" transitions are not pure d-d excitations (*vide supra*),

Table IV. Comparison of Experimental and ZINDO-Derived Molecular Hyperpolarizabilities along the Dipole Moment Direction (β_{vec}) and the ZINDO-Derived Total Intrinsic Hyperpolarizability (β_{tot}) at 1.91 μm ($\hbar\omega = 0.65$ eV) for Various Chromium Arene Derivatives^a


| | Y | $\beta_{\text{vec}}^{\text{expt } b}$ | $\beta_{\text{vec}}^{\text{calc}}$ | $\beta_{\text{tot}}^{\text{calc}}$ | μ_x^{calc} | μ_z^{calc} | $\mu^{\text{expt } b}$ |
|----|----------------------------------|---------------------------------------|------------------------------------|------------------------------------|-----------------------|-----------------------|------------------------|
| 14 | H | -0.8 | -1.30 | 1.30 | 0.0 | 8.6 | 4.4 |
| 15 | OCH ₃ | -0.9 | -1.36 | 1.50 | 0.6 | 8.6 | 4.7 |
| 16 | NH ₂ | -0.6 | -1.27 | 1.42 | 1.1 | 8.8 | 5.5 |
| 17 | N(CH ₃) ₂ | -0.4 | -0.91 | 1.12 | 1.4 | 8.9 | 5.5 |
| 18 | COOCH ₃ | -0.7 | -1.79 | 4.28 | -4.5 | 8.1 | 4.0 |
| 19 | <i>trans</i> -styrenyl | -2.2 | -3.93 | 4.80 | 0.8 | 8.6 | 4.0 |

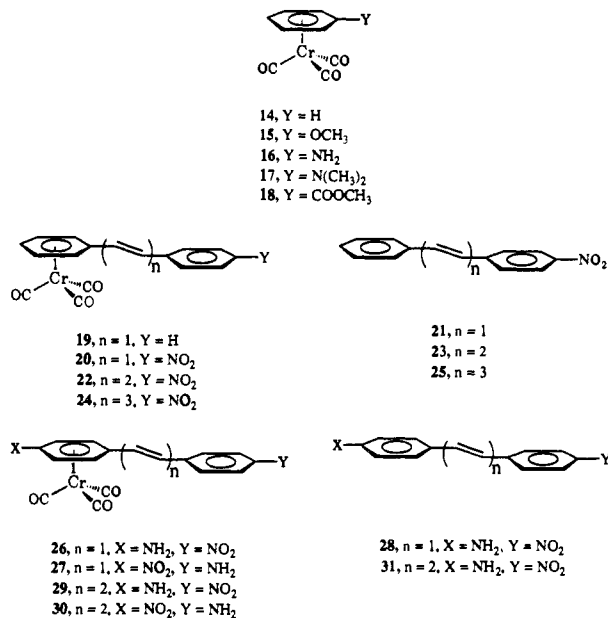
^a Also included is the calculated dipole moment in the x and z directions as defined above. All NLO data are in units of 10^{-30} cm⁵ esu⁻¹; all dipole moment data are in units of debyes. Negative dipole moments are indicative of negative charge buildup in the positive coordinate direction. ^b Dipolar and nonlinear optical data from ref 7.

a small additional contribution to β_{vec} can be anticipated. Unfortunately, the broad LF transitions in the 400–550-nm range, while contributing little to the β , will substantially diminish the useful optical transparency window of ferrocenyl chromophores in this energy region.

The present ZINDO results, in agreement with those in ref 8, show that the metal-containing fragment plays a key role in determining the NLO response in these ferrocenyl chromophores. However, by virtue of the electronic similarities between the ferrocenyl donor and a conventional organic donor, the effect of incorporating the former fragment is both predictable and easily understandable in terms of conventional chromophore design wisdom. Also in accord with the previous work, our results argue for an operational equivalency between the methoxyphenyl donor and the ferrocenyl fragment. However, the methoxyphenyl donor is not an exceptionally potent π -electron donor by organic chromophore standards, and therefore, the magnitudes of the ferrocenyl NLO responses, while large relative to those of most transition-metal-based chromophores,^{7,8} are modest relative to those of efficient π -organic chromophores. Our MO analysis indicates that the iron center *does* efficiently couple to the organic ligand. It is precisely this property that gives the ferrocenyl complexes their organic-like NLO characteristics and leads to the large ferrocenyl β responses relative to those of many other classes of organometallic chromophores (vide infra). For example, the large oscillator strengths observed for these molecules can be directly related to the covalency of the ferrocenyl–ligand interaction, as shown in Figure 8. The ferrocenyl chromophores examined in this section have proven to be readily understandable in terms of traditional chromophore design guidelines. In contrast, most organometallic chromophores studied to date reveal that the ferrocenes are the exception rather than the rule. ZINDO-SOS computations on the chromium arene tricarbonyls identify features unique to organometallic chromophores.

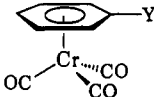
Chromium Arene Derivatives. The next class of molecular chromophores to be investigated are (η^6 -C₆H₆)Cr(CO)₃-based architectures (14–31, Figure 11). These classic organometallic structures are representative of a broad range of transition-metal species containing low-valent metal centers. For this reason, the findings from detailed ZINDO-SOS analyses of chromium arene chromophores should apply to many low-valent organometallic structures. In our discussion, the parent chromium arene (14) will serve as the prototype for this class of chromophores.

Before we discuss the ZINDO-SOS computed responses for the chromium complexes, it is useful to summarize the predominant electronic structure features as given in the literature. The Cr(CO)₃ fragment is generally accepted as a strongly electron-withdrawing fragment in η^6 -arene structures.^{56,57} This charac-

**Figure 11.** Chromium arene chromophores examined in this study along with molecular identification scheme.

teristic is readily seen in metrical parameters⁵⁸ as well as in chemical properties.⁵⁹ Our ZINDO-SOS computations confirm that the Cr(CO)₃ moiety is acting as an electron-withdrawing group in 14. Specifically, the calculated dipole moment of +8.6 D (Table IV) for 14, oriented in the z direction, reveals that the three carbonyl ligands act as electron acceptors in the ground state of (η^6 -C₆H₆)Cr(CO)₃. Previous spectroscopic and theoretical studies have analyzed the dominant excitations in Cr(CO)₃^{57,60,61} and (η^6 -C₆H₆)Cr(CO)₃.^{57,62} The lowest lying MLCT band in the former is assigned to a d_x-to-CO 2 π^* excitation, and the latter is usually assigned to a d_x-to-arene π^* with some admixed d_x-to-CO 2 π^* character.⁵⁷ If this MLCT transition dictates the NLO response in 14, we should expect that β_{vec} will be negative, since the ground-state dipole moment is directed toward the carbonyl ligands while the MLCT band is directed toward the π -C₆H₆ ligand.

(58) Rees, B.; Mitschler, A. *J. Am. Chem. Soc.* **1976**, *98*, 7918–7924.(59) See, for example: Elschenbroich, Ch.; Salzer, A. *Organometallics: A Concise Introduction*; VCH: Weinheim, Germany, 1989.(60) Johnson, J. B.; Klemperer, W. G. *J. Am. Chem. Soc.* **1977**, *99*, 7132–7137.(61) Kotzian, M.; Rösch, N.; Schroder, H.; Zerner, M. C. *J. Am. Chem. Soc.* **1989**, *111*, 7687–7696.(62) (a) Lundquist, R. T.; Cais, M. *J. Org. Chem.* **1962**, *27*, 1167–1172.(b) Yamada, S.; Nakamura, H.; Tshuchida, R. *Bull. Chem. Soc. Jpn.* **1960**, *33*, 481–492.(56) (a) Muetterties, E. L.; Bleeke, J. R.; Wucherer, E. J.; Albright, T. A. *Chem. Rev.* **1982**, *82*, 499–525. (b) Silverthorn, W. E. *Adv. Organomet. Chem.* **1975**, *13*, 47–137.(57) Carroll, D. G.; McGlynn, S. P. *Inorg. Chem.* **1968**, *7*, 1285–1290.

Table V. Comparison of Experimental and ZINDO-Derived Optical Maxima (λ_{max}) and Associated Oscillator Strengths (f) for the Chromium Arene Derivatives^a


| | Y | LF transition | | | MLCT transition | | | λ_{expt}^b |
|----|----------------------------------|-------------------------|------|-------------|-------------------------|------|-------------|---------------------------|
| | | λ^{calc} | f | $\Delta\mu$ | λ^{calc} | f | $\Delta\mu$ | |
| 14 | H | 292 | 0.13 | 1.6 | 225 | 0.60 | 1.9 | 310 |
| 15 | OCH ₃ | 294 | 0.12 | 1.1 | 227 | 0.64 | 1.6 | 310 |
| 16 | NH ₂ | 278 | 0.11 | 0.7 | 230 | 0.52 | 0.8 | 313 |
| 17 | N(CH ₃) ₂ | 278 | 0.11 | 1.2 | 237 | 0.11 | 2.7 | 318 |
| 18 | COOCH ₃ | 273 | 0.12 | 2.0 | 241 | 0.15 | 2.4 | 318 |
| 19 | <i>trans</i> -styrenyl | | | | 337 | 0.14 | 6.1 | 410 |

^aAll energy data are in units of nanometers; all dipole moment data are in units of debyes. ^bSpectroscopic data in toluene from ref 7.

Scheme III. Analysis of β for Molecule 14

| | |
|---|------|
| Two-level contribution ($\beta_{\text{vec},2}$) | -2.4 |
| Three-level contribution ($\beta_{\text{vec},3}$) | 1.1 |
| Total ($\hbar\omega = 0.65$ eV) | -1.3 |
| β_{vec} in units of 10^{-30} cm ⁵ esu ⁻¹ | |

Assumption 1: Three-level terms scale as two-level terms. Therefore, understanding two-level terms will provide qualitative understanding of β .

60% of the total two-level contribution comes from one two-level term involving a MLCT at 225 nm with an oscillator strength of 0.60.

20% of the total two-level contribution comes from another two-level term involving a ligand-field transition at 292 nm with an oscillator strength of 0.13.

Assumption 2: The two-level contribution is dominated by two excited states. Therefore, understanding these excited states will provide a qualitative understanding of β .

Experimental nonlinear optical response data are available for six arene-Cr(CO)₃ chromophores (14–19).⁷ As shown in Table IV, the ZINDO-derived susceptibilities are in excellent agreement with EFISH results, with theory and experiment finding that all six chromophores possess negative second-order susceptibilities in accordance with our predictions. Note, however, that the magnitudes of β_{vec} for the arene chromophores are an order of magnitude smaller than those of the aforementioned ferrocenyl derivatives and two orders of magnitude less than those of the most efficient organic chromophores. In the discussion below, we will analyze the origin of these low quadratic hyperpolarizabilities and suggest presently unrealized arene-based molecular architectures for which the ZINDO model predicts large NLO responses.

A priori, one possible source for the relatively small β_{vec} values in the arene-Cr(CO)₃ chromophores is that the charge-transfer excitation is not directed along the ground-state dipole moment axis (i.e., $\beta_{\text{vec}} \ll \beta_{\text{tot}}$). As shown in Table IV, however, the majority of β_{tot} (>75%) is collinear with the dipole direction for the six chromophores with the exception of chromophore 18, where less than 50% of the intrinsic nonlinearity will be sampled by EFISH. Clearly, the inherently small NLO responses for this class of molecules are of electronic origin. The quantum chemical information provided by the ZINDO-SOS algorithm permits an understanding of the electronic features limiting β_{vec} in these structures.

As shown in Scheme III, the two-level contributions in the arene prototype 14 are approximately twice the three-level contributions and of opposite sign, in accord with the aforementioned observations for most chromophores. Thus, we have again reduced the nonlinear optical computations to an understanding of the linear optical characteristics. We note that a ZINDO study of the linear optical properties of the closely related molecule Cr(CO)₆ has recently appeared.⁶¹ The authors find the ZINDO-derived optical characteristics of Cr(CO)₆ to be in excellent agreement with the gas-phase optical data. The experimental and theoretical spectral features for Cr(CO)₆ both include a highly allowed excitation in the UV near 225 nm. Interestingly, the chromium arenes also possess intense MLCT bands in the near-UV yet are found to have

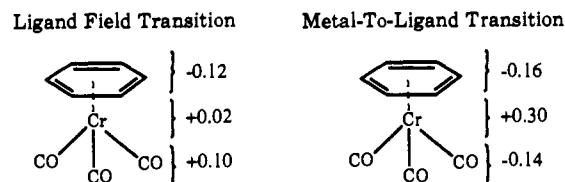


Figure 12. The difference in electronic populations between ground state and two crucial excited states for the prototypical chromium arene derivative (14) as determined by ZINDO calculations. A negative population reflects an increase in electron density in the charge-transfer process.

very small nonlinear optical responses.

As indicated in Scheme III, two transitions dictate the NLO response of 14 within the framework of the SOS formalism. The lower energy transition ($\lambda = 292$ nm, $f = 0.13$) comprises 20% (-0.5×10^{-30} cm⁵ esu⁻¹) of the total two-level contribution. As depicted in Figure 12, this excitation involves a small charge transfer from the carbonyl ligands to the arene fragment. However, obscured from the charge analysis is that 0.40 Cr d_x electrons are promoted into Cr d_z orbitals. As anticipated, the oscillator strength associated with such a Laporte-forbidden, ligand-field transition is small and the resulting contribution to the NLO response from this excitation is small on an absolute scale. The higher energy excitation ($\lambda = 225$ nm, $f = 0.60$) is responsible for 60% (-1.5×10^{-30} cm⁵ esu⁻¹) of the two-level contribution to β_{vec} . The magnitude of this dominant MLCT contribution to β_{vec} is significantly less than that for the representative ferrocenyl chromophore (14, -1.5×10^{-30} cm⁵ esu⁻¹; 3, 54.5×10^{-30} cm⁵ esu⁻¹). Clearly, the relatively small second-order responses observed for 14–19 are due to the modest contributions from the MLCT excitations.

As shown in Table V, the MLCT transition for chromophore 14 is calculated to be found at 225 nm. Note, however, that this highly allowed transition is observed experimentally at 310 nm, somewhat red-shifted from the ZINDO-derived energy. The computed absorption energy is also slightly red-shifted in chromophores 15–19. Our computations suggest that this excitation is extremely sensitive to the exact choice of Cr–CO and C–O bond lengths, and this could be the origin of the disparity between theory and experiment. Nevertheless, the ZINDO results provide great insight into the origin of NLO activity in these chromophores (vide infra).

If the three ZINDO-derived crucial optical parameters (f , λ , $\Delta\mu$) for the dominant MLCT in the prototypical ferrocenyl (3) and arene (14) chromophores are analyzed, the computed oscillator strengths are comparable (3, 0.90; 14, 0.60), the calculated λ of the transition is red-shifted in 3 (354 nm) relative to 14 (225 nm), and most significantly, there is a major disparity in the change in dipole moments computed for the respective MLCT transitions (3, 14.1 D; 14, 1.9 D). Figure 12 shows the difference in regional charge between ground state and appropriate excited state for 14. Note that significant electron density (0.30 electrons) is transferred to the π -ligands in this MLCT transition. However, the

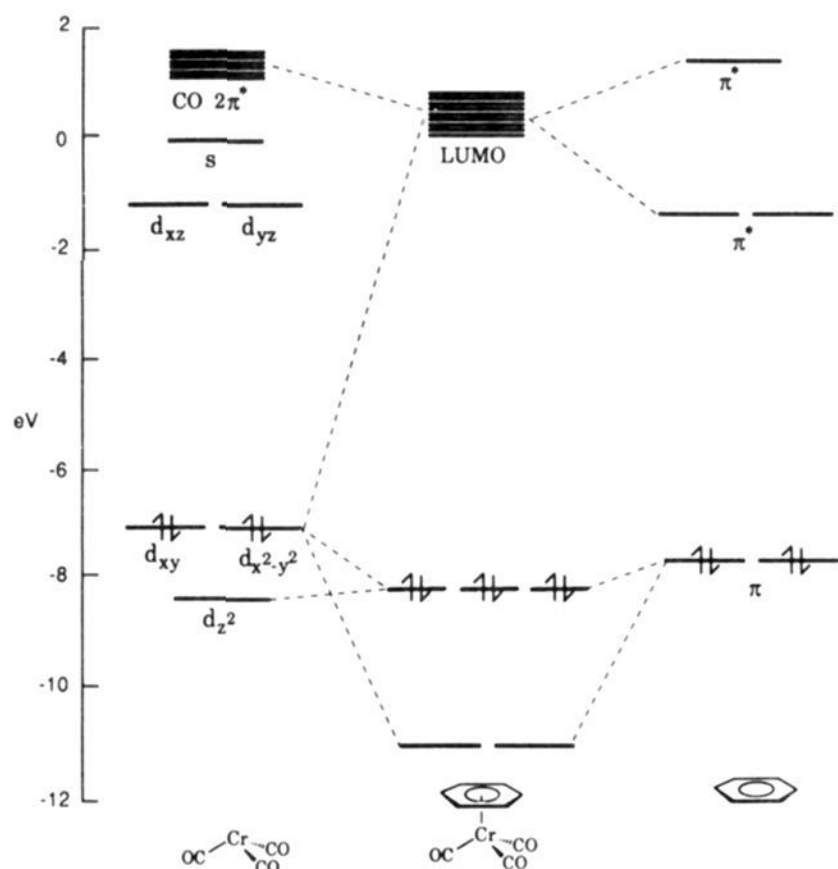


Figure 13. Molecular orbital diagram for the representative chromium arene chromophore (**14**). The $\text{Cr}(\text{CO})_3$ fragment labels represent the Cr or CO orbitals that dominate a given $\text{Cr}(\text{CO})_3$ fragment orbital.

charge-transfer electron density is nearly equally divided between the carbonyl and arene ligands. As a consequence, only a modest $\Delta\mu$ is associated with this d_x -ligand π^* transition, and this ultimately limits the quadratic hyperpolarizability in **14**.

The MLCT transition in **14** cannot be represented by a single excitation between an occupied and unoccupied molecular orbital. Rather, several configuration excitations participate in the MLCT absorption. This transition can be understood from the ZINDO-derived MO diagram for $(\eta^6\text{-C}_6\text{H}_6)\text{Cr}(\text{CO})_3$ (Figure 13). In this diagram, we have chosen to partition the molecule into a $\text{Cr}(\text{CO})_3$ fragment and a benzene moiety. The frontier molecular orbitals of both fragments have been discussed previously.⁶³ The fragment orbital labels for $\text{Cr}(\text{CO})_3$ appearing in Figure 13 reflect the dominant atomic character of a particular fragment orbital. For example, the Cr " d_x " orbitals possess some CO character. The ligand orbital combinations are deliberately simplified in this MO diagram. Specifically, the six CO π^* orbitals and the three C_6H_6 π^* ligand orbitals are all depicted as one "LUMO". Since many of the transitions from the d_x orbitals into the ligand π^* orbitals are Laporte-allowed, a number of these configuration transitions make modest contribution to β_{vec} through the MLCT transition and therefore greatly complicate our simple picture. Perhaps the most important observation from this MO diagram is that there is significant mixing between the arene π^* and the CO $2\pi^*$ orbitals, resulting in unfilled molecular orbitals containing substantial arene and CO character. Note that only two of the three Cr d_x orbitals are forced to be degenerate for symmetry reasons. The near degeneracy of the third metal π -orbital with the other two reflects the pronounced pseudo-octahedral electronic symmetry of this chromophore.

From the NLO (Table IV) and linear optical (Table V) data for chromophores **15–19**, it is clear that the above conclusions for **14** are applicable to other chromium arene structures irrespective of arene ring derivatization. Specifically, the $\Delta\mu$ values calculated for all the six arene chromophores are far below the 15–20 D computed for high- β organic or ferrocenyl chromophores. Therefore, even though some of the oscillator strengths calculated for the dominant MLCT in these molecules are reasonably large, the electronic pseudosymmetry dictates that their NLO responses will be small. Note that even though the computed energy of the CT excitation may be somewhat blue-shifted relative to experi-

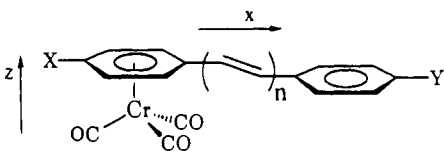
ment, the electronic asymmetry between the two ligands is related to the difference in orbital energies between the two sets of π -ligands and should therefore be obtained regardless of the disparity between observed and computed λ .

The general trend in the computed and experimental β values (Table IV) is rationalized as follows. Since the ground-state dipole moment is essentially unaffected by derivatization of the η^6 -benzene ring (Table IV), it is always directed toward the CO ligands. In addition, the MLCT direction is always slightly skewed toward the arene ring; thus, the antiparallel nature of the ground-state dipole moment and the charge-transfer direction dictates that β will be negative for chromophores **14–19**. When an electron-withdrawing substituent (**18**, **19**) is appended to the arene ring, the orbital energy of the arene- π^* orbital is lowered, thereby red-shifting the MLCT transition and increasing β_{tot} . Electron-donating substituents will clearly have the opposite effect, thereby decreasing the second-order NLO response. Recall that the calculated value of β_{tot} , the intrinsic NLO susceptibility, is positive by definition. Note that the smallest β_{tot} is calculated for the molecule with the strongest donor (**17**, $1.12 \times 10^{-30} \text{ cm}^5 \text{ esu}^{-1}$), while the largest values of β_{tot} are predicted for the strongest acceptors (**18**, $4.28 \times 10^{-30} \text{ cm}^5 \text{ esu}^{-1}$; **19**, $4.80 \times 10^{-30} \text{ cm}^5 \text{ esu}^{-1}$). However, the calculated and experimental β_{vec} values for **18** are nearly equal to those of **14–17** rather than **19**. As illustrated by its ground-state dipole moment, the charge-transfer direction (z) is not parallel to the dipole moment direction (x and z) in **18**. Therefore, the EFISH and ZINDO-derived β_{vec} values ($-0.7 \times 10^{-30} \text{ cm}^5 \text{ esu}^{-1}$ and $-1.79 \times 10^{-30} \text{ cm}^5 \text{ esu}^{-1}$, respectively) are somewhat smaller in magnitude than the computed total susceptibility ($4.28 \times 10^{-30} \text{ cm}^5 \text{ esu}^{-1}$) (Table IV). Overall, however, chromophores **14–19** all display pseudo-octahedral electronic symmetry about the metal and therefore exhibit very small NLO responses irrespective of the substituents attached to the arene ring.

The obvious prescription for enhancing β_{vec} via exploitation of the highly allowed charge-transfer transitions observed for the chromium tricarbonyl complexes would be to remove the aforementioned electronic pseudosymmetry. One potential solution would increase the π -conjugation length in the organic arene ligand, in analogy to the 1-ferrocenylethylene chromophores. For this purpose, ZINDO-SOS NLO response calculations were carried out on hypothetical arene chromophores **20**, **22**, **24**, **26**, **27**, **29**, and **30** and the organic analogues **21**, **23**, **25**, **28**, and **31**. Three points are readily apparent from the theoretical results reported in Table VI: (1) the β_{vec} values for the hypothetical arene complexes are significantly *less* than those in the $\text{Cr}(\text{CO})_3$ -free analogues, (2) the computed β_{vec} values are markedly *less* than the β_{tot} values for all hypothetical $\text{Cr}(\text{CO})_3$ -derivatized chromophores examined, and (3) the β_{vec} values are *positive* for these arene molecules, in direct contrast to the negative quadratic hyperpolarizabilities found for chromophores **14–19**. These unexpected results will serve to illustrate some of the potential problems associated with organometallic chromophores in general.

When electronically "inert" d electrons are involved in the MLCT transition that dictates β (within the SOS formalism), there is a question as to whether the total second-order nonlinearity (β_{tot}) will, in fact, be sampled by EFISH (β_{vec}). That is, the principal charge-transfer direction may not coincide with the ground-state dipole moment direction. This is not a concern in most organic systems where orbitals that dictate the ground-state dipole moment are almost invariably involved in the primary π to π^* charge-transfer transition. However, in the arene complexes of interest here, the electron density of all occupied molecular orbitals (i.e., dipole moment) indicates that there is a charge buildup on the carbonyl fragments in the z direction. As anticipated, altering the arene substituents in **14–31** has essentially no effect on the magnitude of μ_z , as reported in Tables IV and VI. What will change, however, is the magnitude of μ_x as the arene fragment is derivatized with better acceptors or modified to afford increased π -delocalization lengths. In molecule **20**, for example, $\mu_z = 8.4 \text{ D}$ and $\mu_x = -6.6 \text{ D}$. In contrast, the ferrocenyl chromophores of the previous section have very small μ_z compo-

(63) Albright, T. A.; Burdett, J. K.; Whangbo, M. H. *Orbital Interactions in Chemistry*; Wiley: New York, 1985.

Table VI. ZINDO-Derived Molecular Hyperpolarizabilities along the Dipole Moment Direction (β_{vec}) and ZINDO-Derived Total Intrinsic Hyperpolarizabilities (β_{tot}) at 1.91 μm ($\hbar\omega = 0.65$ eV) for Hypothetical Chromium Arene Derivatives^a


| | X | Y | n | | $\beta_{\text{vec}}^{\text{calc}}$ | $\beta_{\text{tot}}^{\text{calc}}$ | μ_x^{calc} | μ_z^{calc} |
|----|-----------------|-----------------|---|----|------------------------------------|------------------------------------|-----------------------|-----------------------|
| 20 | H | NO ₂ | 1 | Cr | 8.3 | 23.5 | -6.6 | 8.4 |
| 21 | H | NO ₂ | 1 | | 27.5 | 27.5 | -7.5 | 0.0 |
| 22 | H | NO ₂ | 2 | Cr | 11.5 | 28.4 | -6.7 | 8.5 |
| 23 | H | NO ₂ | 2 | | 41.9 | 42.0 | -7.8 | 0.0 |
| 24 | H | NO ₂ | 3 | Cr | 15.6 | 34.5 | -6.8 | 8.6 |
| 25 | H | NO ₂ | 3 | | 57.6 | 57.9 | -8.1 | 0.0 |
| 26 | NH ₂ | NO ₂ | 1 | Cr | 10.7 | 23.6 | -7.8 | 8.7 |
| 27 | NO ₂ | NH ₂ | 1 | Cr | 14.8 | 26.6 | 8.8 | 7.3 |
| 28 | NH ₂ | NO ₂ | 1 | | 46.4 | 46.5 | -9.5 | 0.0 |
| 29 | NH ₂ | NO ₂ | 2 | Cr | 16.2 | 31.2 | -8.0 | 8.8 |
| 30 | NO ₂ | NH ₂ | 2 | Cr | 27.5 | 41.4 | 9.2 | 7.3 |
| 31 | NH ₂ | NO ₂ | 2 | | 65.7 | 65.9 | -9.8 | 0.0 |

^a Also included is the calculated dipole moment in the x and z directions as defined above. All NLO data are in units of 10^{-30} $\text{cm}^5 \text{esu}^{-1}$; all dipole moment data are in units of debyes. A "Cr" designation indicates that the chromophore contains a $\text{Cr}(\text{CO})_3$ moiety in the indicated position; no designation is indicative of a metal-free ligand.

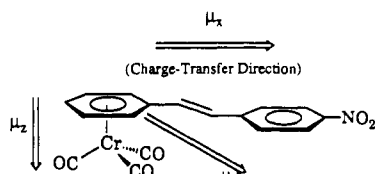


Figure 14. Figure displaying the noncoincidence of ground-state dipole moment direction and principal charge-transfer direction in **20**. The arrows are directed toward areas of increased electron density.

nents (Table I), and therefore $\mu_x \sim \mu_{\text{tot}}$ and $\beta_{\text{vec}} \sim \beta_{\text{tot}}$. As shown schematically in Figure 14, the dipole direction in **20** bisects the x and z directions, while the primary charge-transfer direction is in the arene xy plane. For this reason, the ZINDO-SOS results suggest that only 30% of the NLO response of **20** ($\beta_{\text{tot}} = 23.5 \times 10^{-30}$ $\text{cm}^5 \text{esu}^{-1}$, $\beta_{\text{vec}} = 8.3 \times 10^{-30}$ $\text{cm}^5 \text{esu}^{-1}$) will be observable in EFISH experiments.⁶⁴

The positive second-order susceptibilities for the hypothetical arene chromophores listed in Table VI also provide insight into the electronic origin of the NLO response in these structures. From the previous discussion, any NLO component in the z direction should possess a negative β_{vec} . In contrast, the dipole moment in the arene plane is directed toward the NO_2 moiety, as is the charge-transfer direction. In analogy to the case of the ferrocenyl chromophores or traditional donor-acceptor π -organics, the β component within the arene plane should therefore be positive. That the ZINDO-SOS-derived β_{vec} responses for these hypothetical chromophores are invariably positive provides strong evidence that x is the charge-transfer direction and not z as for chromophores **14**–**19**.

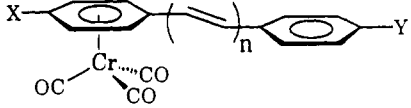
The ZINDO-SOS results (Table VI) show that the metal-free molecules (**21**, **23**, **25**, **28**, **31**) possess larger NLO responses (β_{tot}) than the corresponding metal-complexed structures. For example, the computed β_{tot} for the $n = 3$ metal-free arene (**24**, 57.9×10^{-30} $\text{cm}^5 \text{esu}^{-1}$) is significantly enhanced relative to the $\text{Cr}(\text{CO})_3$ -coordinated chromophore (**25**, 34.5×10^{-30} $\text{cm}^5 \text{esu}^{-1}$). In the metal-free structures **21**, **23**, and **25**, the unsubstituted phenyl group acts as a weak donor coupled through the π -backbone to the nitro acceptor to afford only modest second-order responses.

Complexing the fragment reduces the intrinsic nonlinearity and lowers the calculated β_{vec} due to the aforementioned dipole moment problem. As the conjugation length in the $\text{Cr}(\text{CO})_3$ -coordinated molecules is increased from $n = 1$ through $n = 3$, the computations indicate that only a modest increase in β_{tot} is observed (23.5×10^{-30} $\text{cm}^5 \text{esu}^{-1}$ for $n = 1$; 34.5×10^{-30} $\text{cm}^5 \text{esu}^{-1}$ for $n = 3$), while the analogous metal-free chromophores behave as conventional organic structures with an increasing β_{vec} ($\sim \beta_{\text{tot}}$) from 27.5×10^{-30} $\text{cm}^5 \text{esu}^{-1}$ for **21** to 57.9×10^{-30} $\text{cm}^5 \text{esu}^{-1}$ for **25**. In addition, if we take reasonable donor-acceptor chromophores and functionalize one of the aromatic rings with a $\text{Cr}(\text{CO})_3$ group, the computed optical nonlinearity drops significantly regardless of which ring is functionalized, as shown in Table VI for molecules **26**, **27**, **29**, and **30**. Ironically, if the $\text{Cr}(\text{CO})_3$ group is coordinated to either an acceptor- or donor-function-based phenyl ring, the effect on β is virtually the same.

The hypothetical arene chromophore with three ethylenic units (**24**) fits within the two-level model and offers the possibility of a detailed delineation of the computed quadratic hyperpolarizability. Specifically, the ZINDO-derived two-level contribution for **24** ($\beta_{\text{vec},2} = 42.4 \times 10^{-30}$ $\text{cm}^5 \text{esu}^{-1}$) is nearly twice the three-level contribution ($\beta_{\text{vec},3} = -26.9 \times 10^{-30}$ $\text{cm}^5 \text{esu}^{-1}$), in accord with results for most other nonlinear optiphoric structures. Approximately 70% of the total two-level contributions derives from one excitation, the MLCT described in Table VII. The metal-free analogue of **24** and **25** also fits the two-level descriptions, and one charge-transfer transition dominates the NLO response.

Details of the dominant charge-transfer transitions in **24** and **25** are given by the change in electron density associated with the dominant excitation (Figure 15). The excited state is localized on the nitro group in both chromophores; however, the nitro substituent gains more electron density (i.e., charge transfer is greater) in the metal-free chromophore than with the $\text{Cr}(\text{CO})_3$ group attached. Specifically the phenyl- NO_2 acceptor moiety gains 0.57 electrons in the isolated ligand via a LLCT and only 0.47 electrons using the MLCT in the arene derivative. The computed $\Delta\mu$ values given in Table VII for the metal-complexed (8.2 D) versus the metal-free (12.6 D) chromophore are in agreement with the results from Figure 15. The data in Table VII indicate that converting the LLCT in the organic arene into a MLCT by adding an $\text{Cr}(\text{CO})_3$ moiety will universally decrease $\Delta\mu$ by 30–70%. From Table VII, we see that the calculated λ_{max} of **24** and **25** are essentially identical (~ 395 nm); however the oscillator strength for the metal-free molecule (1.86) is somewhat greater than that for the metal-complexed molecule (1.45). Thus, complexing the $\text{Cr}(\text{CO})_3$ fragment to an organic ligand will decrease the magnitude of the charge transfer and decrease the

(64) Note that the computed responses for the arene chromophores given in Table VI are very sensitive to metrical input parameters, particularly the Cr-CO distances. Nevertheless, for any reasonable choices of metrical parameters, the qualitative conclusion remains the same: an η^6 coordination of a $\text{Cr}(\text{CO})_3$ fragment induces a ground-state dipole component perpendicular to the MLCT direction if introduced into an extended organic π -electron system.

Table VII. Comparison of Experimental and ZINDO-Derived Optical Maxima (λ_{max}) and Associated Oscillator Strengths (f) for Several Chromium Arene Derivatives^a


| | X | Y | n | | MLCT transition | | |
|----|-----------------|-----------------|---|----|-------------------------|------|-------------|
| | | | | | λ^{calc} | f | $\Delta\mu$ |
| 20 | H | NO ₂ | 1 | Cr | 368 | 0.24 | 9.2 |
| 21 | H | NO ₂ | 1 | | 355 | 1.13 | 12.8 |
| 24 | H | NO ₂ | 3 | Cr | 393 | 1.45 | 8.2 |
| 25 | H | NO ₂ | 3 | | 398 | 1.86 | 12.6 |
| 26 | NH ₂ | NO ₂ | 1 | Cr | 376 | 0.14 | 6.5 |
| 27 | NO ₂ | NH ₂ | 1 | Cr | 345 | 1.45 | 6.8 |
| 28 | NO ₂ | NH ₂ | 1 | | 375 | 1.19 | 14.8 |

^aAll energy data are in units of nanometers. A "Cr" designation indicates that the chromophore contains a Cr(CO)₃ moiety in the indicated position; no designation is indicative of the a metal-free ligand with no Cr(CO)₃ group attached.

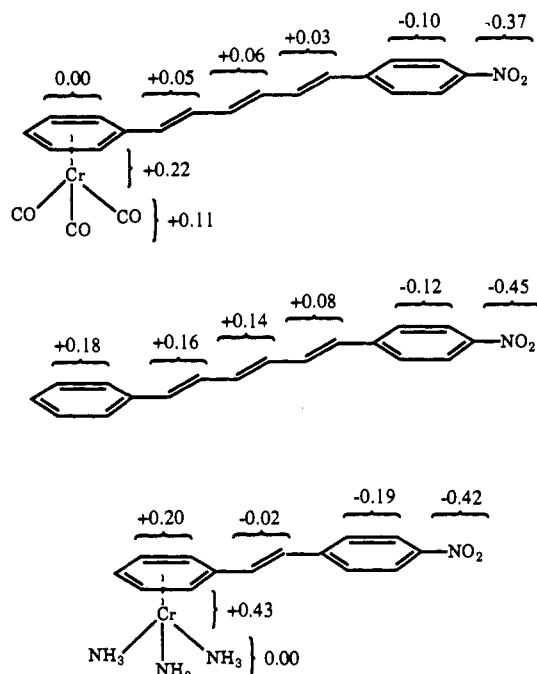


Figure 15. The difference in electronic populations between ground state and β -dominating excited state for Cr(CO)₃-arene derivative (**24**), the metal-free arene (**25**), and a Cr(NH₃)₃-arene derivative (**32**), as calculated by ZINDO. A negative population reflects an increase in electron density in the charge-transfer process.

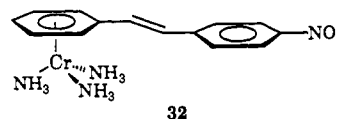
oscillator strength of the β -dominating transition.

The mechanism of charge transfer for (η^6 -C₆H₅-(C₂H₂)₃-C₆H₄-NO₂)Cr(CO)₃ can be probed further by examining the ZINDO-derived molecular orbital diagram for the prototypical chromophore (Figure 16). The dominant charge-transfer excitation in this chromophore, as computed through configuration interaction, is found to be 60% HOMO \rightarrow LUMO and 25% HOMO \rightarrow SLUMO. Since the energy and orbital makeup of the LUMO and SLUMO are virtually identical, we will focus on the orbital origin of the HOMO \rightarrow LUMO excitation. As for the ferrocenyl derivatives, there is a strong covalent interaction between the $d_{xz,yz}$ orbital and the arene π -system which serves to break the degeneracy of the three d_x orbitals (i.e., destroy the octahedral pseudosymmetry about the metal). The calculations also suggest that the LUMO and SLUMO are predominantly localized on the arene ligand, in contrast to the (η^6 -C₆H₆)Cr(CO)₃ (**14**) LUMO, which contains nearly equal amounts of arene and CO character. As a consequence, the charge-transfer excitation is much more unidirectional in **24** than in **14**, as evidenced by the larger values of $\Delta\mu$. In the isolated ligand, the HOMO \rightarrow LUMO ($\pi \rightarrow \pi^*$) transition dictates the second-order NLO response. From Figure 16, we see that the energy of the HOMO \rightarrow LUMO

transition in the metal complex is nearly identical to that of the $\pi \rightarrow \pi^*$ transition calculated for the metal-free ligand, in agreement with the similarities in the optical absorption energies for the two chromophores (Table VII). In summary, we can state that the electronic origin of the second-order response in this class of arene chromophores is very similar to that found for the ferrocenyl derivatives. A covalent interaction between the organic ligand and the metal fragment creates an asymmetric environment about the chromium atom, leading to modest second-order responses. From the computed β data in Table VI, it is clear that the inherent responses (β_{tot}) in Cr(CO)₃-substituted organic structures are lower than those in their metal-free organic analogues due to the low $\Delta\mu$ values associated with the dominant charge-transfer excitation. Essentially, the CO ligands are weak acceptors which reduce the donating strength of the d_x orbitals in the chromium arene chromophores. Therefore, even very asymmetric metal-arene structures are not nearly as asymmetric as conventional organic structures. In addition, the noncoincidence of the ground-state dipole moment and the charge-transfer directions dictates that significant portions of the modest second-order responses in this class of chromophores will not be sampled with EFISH nor would conventional poling techniques achieve optimum $\chi^{(2)}$ values for polymer matrices containing these chromophores.

It is apparent that the above features are serious drawbacks to using this class of organometallic chromophores in NLO materials. Moreover, it is clear that these shortcomings will not be limited to this particular class of organometallic structures. As stated previously, it is not uncommon for an MLCT transition originating from a relatively nonbonding d_x orbital to be non-parallel to the ground-state dipole moment direction. In regard to the more serious second shortcoming of the arene complexes, the small $\Delta\mu$ values associated with the MLCT excitations, these should also be representative of most organometallic chromophores where the metal is strongly coupled to the organic ligand. This can be seen by noting that the ligands surrounding a metal center usually reflect the electronic characteristics of the metal center. Hard ligands (NH₃, H₂O, oxides, sulfides) are preferentially coordinated to highly oxidized metal centers, while soft ligands (CO, CN, C₆H₆) prefer reduced centers. In a low-valent environment, for example, the degree of π -basicity can be varied to create a somewhat asymmetric environment; however, substituting one soft base for another will only lead to small $\Delta\mu$ values and modest NLO responses. To truly destroy the electronic pseudosymmetry about a metal center, hard ligands must be coordinated trans to soft ligands about the metal center.

To test this hypothesis, we computed the NLO response for a molecule conforming to the above specifications (**32**). Specifically,



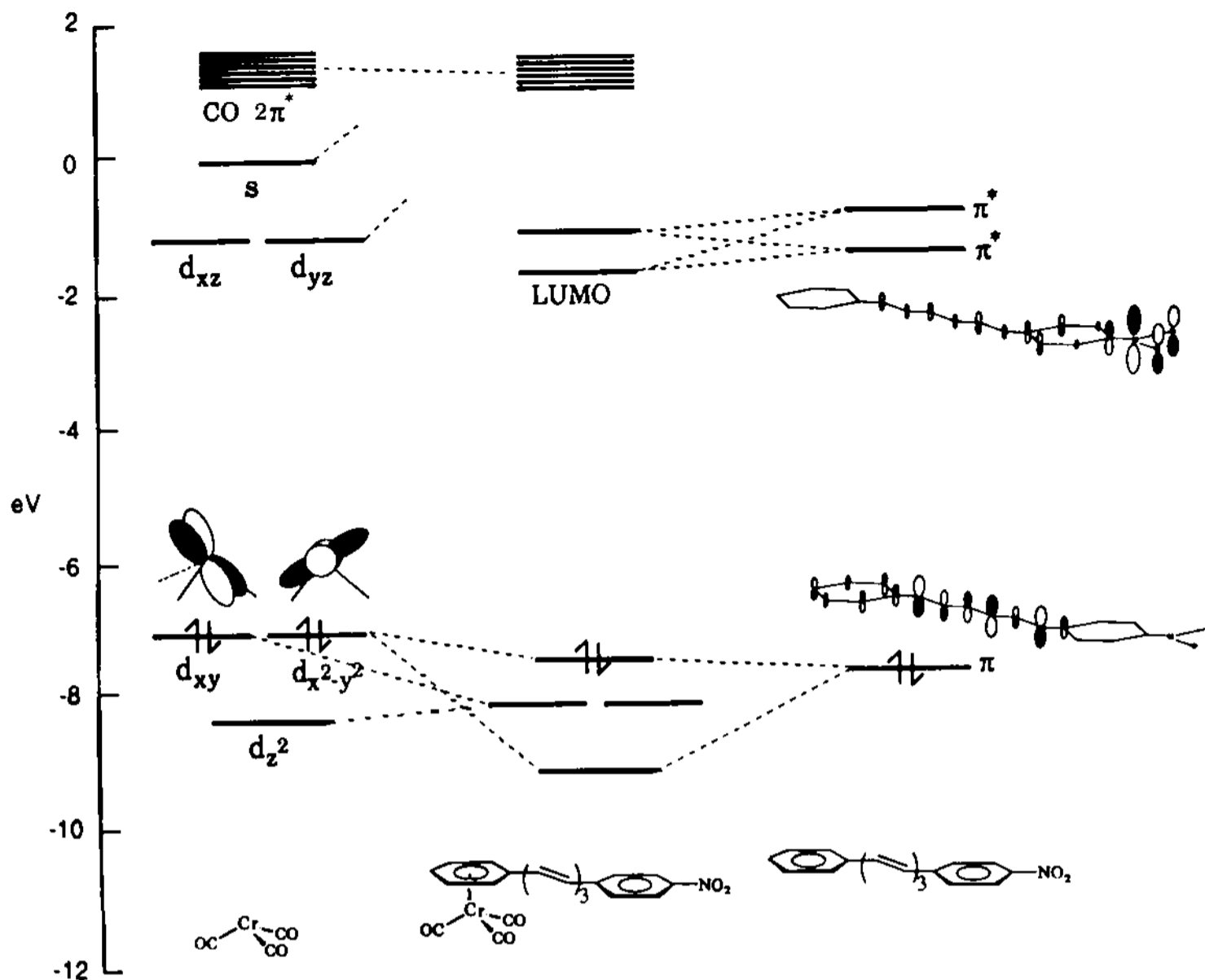


Figure 16. Molecular orbital diagram for 24. The $\text{Cr}(\text{CO})_3$ fragment labels represent the Cr or CO orbitals that dominate a given $\text{Cr}(\text{CO})_3$ fragment orbital.

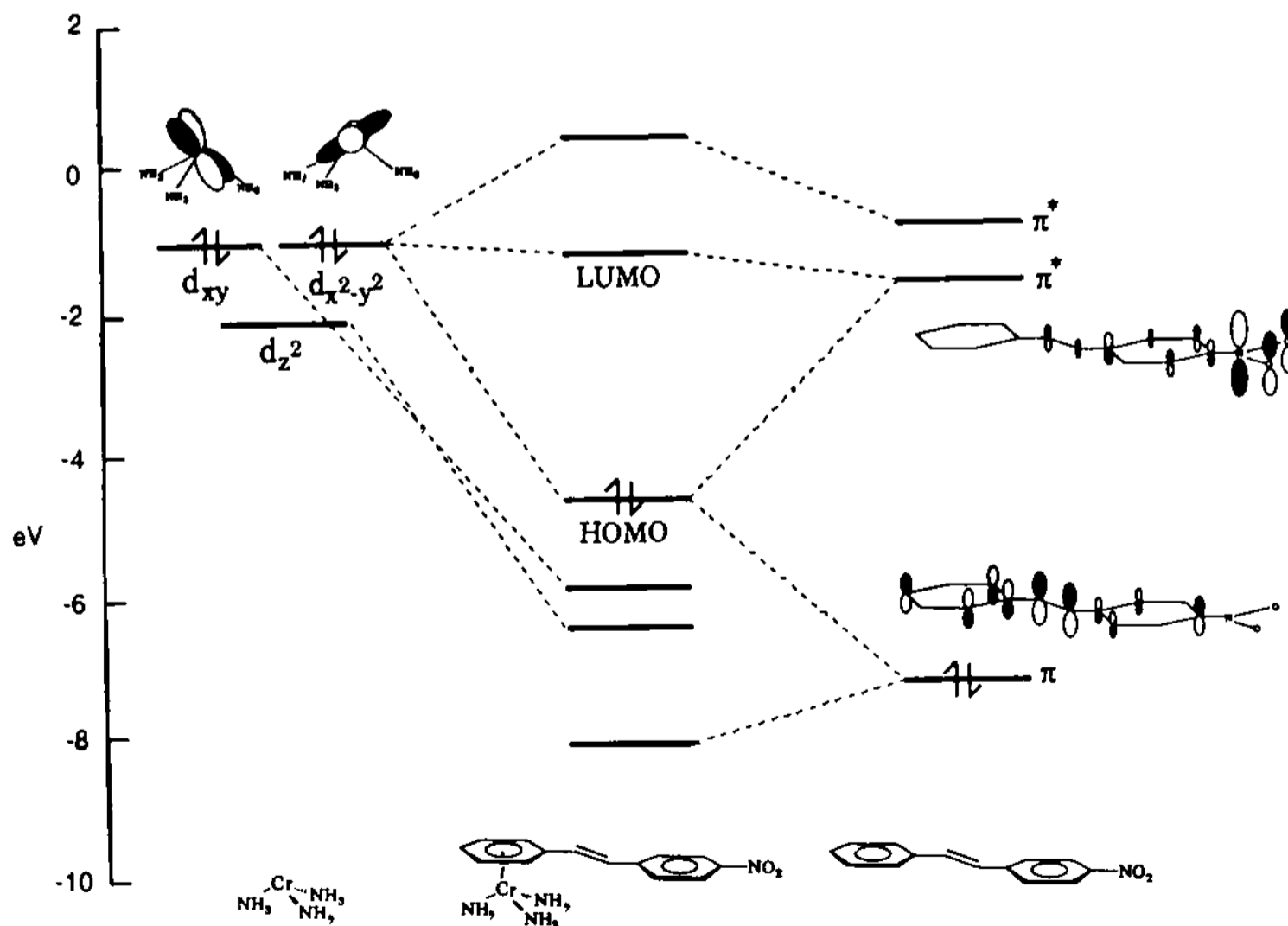


Figure 17. Molecular orbital diagram for chromophore 32. The $\text{Cr}(\text{NH}_3)_3$ fragment labels represent the Cr atomic orbitals that dominate a given $\text{Cr}(\text{NH}_3)_3$ fragment orbital.

a reduced Cr center is surrounded with both hard, electron-releasing NH_3 ligands and a soft arene ligand. Essentially, three

amine ligands are substituted for the three "NLO-inactive" π -accepting CO ligands in chromophore 20. While 32 is strictly

a hypothetical molecule, it illustrates the potential of including hard and soft ligands around a metal center. The ZINDO-derived β_{vec} for **32** is $780 \times 10^{-30} \text{ cm}^5 \text{ esu}^{-1}$ at $\hbar\omega = 0.65 \text{ eV}$, a very large second-order response. In fact, the computed quadratic hyperpolarizability for **32** rivals the largest quadratic hyperpolarizabilities reported for any conventional organic chromophore. A sizeable portion of β_{vec} for **32** is resonance-enhanced due to a 757-nm charge-transfer transition; however, note that the static value of β_{vec} ($\hbar\omega = 0.0 \text{ eV}$) of $245 \times 10^{-30} \text{ cm}^5 \text{ esu}^{-1}$ rivals or exceeds any β_{static} computed to date for a conventional organic chromophore. By comparing the computed response (β_{vec} ($\hbar\omega = 0.65 \text{ eV}$)) of **32** ($780 \times 10^{-30} \text{ cm}^5 \text{ esu}^{-1}$) to that of the metal-free ligand (**21**, $27.5 \times 10^{-30} \text{ cm}^5 \text{ esu}^{-1}$) and the analogous $\text{Cr}(\text{CO})_3$ structure (**20**, $8.3 \times 10^{-30} \text{ cm}^5 \text{ esu}^{-1}$), we see that the $\text{Cr}(\text{NH}_3)_3$ derivatization *significantly* enhances the NLO properties of an arene fragment, while a coordinated $\text{Cr}(\text{CO})_3$ moiety acts as a detriment. The $\text{Cr}(\text{NH}_3)_3$ -appended chromophore fits our empirical two-level model, and therefore an analysis of the dominant charge-transfer transition will provide a detailed understanding of the electronic origin of the NLO response in this novel molecule.

The transition dictating the second-order response of **32** is calculated to be at 757 nm with an oscillator strength of 0.45 and a $\Delta\mu$ of 15.6 D. In contrast to the case of the $\text{Cr}(\text{CO})_3$ -coordinated arenes, the important optical transition in **32** possesses a large charge-transfer component. The population redistribution associated with the charge-transfer transition (Figure 15) rationalizes the computed value for $\Delta\mu$. These electron density differences show that more metal electrons are involved in the charge-transfer excitation in **32** than in a related $\text{Cr}(\text{CO})_3$ -functionalized arene molecule, suggesting that $\text{Cr}(\text{NH}_3)_3$ is acting as a stronger donor than $\text{Cr}(\text{CO})_3$. The energetics of the computed optical excitation can be explained from the MO diagram of **32** (Figure 17), since most of the dominant charge-transfer transition (>85%) is HOMO \rightarrow LUMO. The interaction picture shows that the orbital energies of the metal d_x orbitals are raised significantly relative to the energies found in $\text{Cr}(\text{CO})_3$ arenes due the presence of electron-releasing NH_3 ligands. In fact, they are now at energies comparable with those of the ligand π^* orbitals rather than the π orbitals as was true for all ferrocenyl and $\text{Cr}(\text{CO})_3$ derivatives. The presence of such a high-lying filled set of metal orbitals makes the $\text{Cr}(\text{NH}_3)_3$ fragment a superb donor. The $d_{x^2-y^2}$ metal orbital is the key metal function involved in the bonding interaction. It interacts with both the filled and unfilled frontier orbitals of the

metal-free fragment to form the HOMO and LUMO of the complex. As anticipated, the three d_x orbitals are removed from one another energetically, reflecting the large electronic asymmetry in **32**. In addition, we see that the ground-state dipole moment in the z direction is now directed toward the arene ($\mu_z = -12.70$ in **32**, $\mu_z = 8.4 \text{ D}$ in the $\text{Cr}(\text{CO})_3$ analogue **20**) by virtue of the strongly donating ammine ligands. Thus a much larger percentage of the intrinsic β would be sampled by EFISH in the $\text{Cr}(\text{NH}_3)_3$ -substituted chromophore ($\sim 80\%$ in **32**) than in one of the $\text{Cr}(\text{CO})_3$ derivatives.

Conclusions

Our calculations suggest that if organometallic chromophores are to compete with conventional π -electron donor-acceptor molecules as building blocks for macroscopic second-order NLO materials, the strongly coupled ligation sphere around a given metal must be highly polarized. Only in a very asymmetric environment will the schematic representation (Figure 1) of enhanced NLO responses via organometallic architectures be realized. Unfortunately, most stable organometallic molecules tend to possess electronic pseudosymmetry, and therefore the MLCT transitions one would wish to exploit for NLO responses will not possess significant, unidirectional charge-transfer character.

Perhaps the most important conclusion from this contribution is that efficient quantum chemical methods can be used to understand molecular quadratic hyperpolarizabilities in terms familiar to practicing chemists. These conclusions can then be employed to design new chromophoric units possessing optimal NLO characteristics, and such efforts are continuing in our laboratories. Future publications will address exploiting LMCT excitations, exploiting MLCT transitions in η^1 -coordinated structures, using novel conjugation architectures in potential NLO chromophores, as well as discussing the role of three-level contributions in the NLO response.

Acknowledgment. This research was supported by the NSF-MRL Program through the Materials Research Center of Northwestern University (Grant DMR8821571) and by the Air Force Office of Scientific Research (Contract 90-0071). We thank Professor Michael Zerner for graciously supplying us the ZINDO program and the Pittsburgh Computing Center and Cray Research Inc. for providing supercomputing resources. We also thank Drs. G. R. Meredith, L.-T. Cheng, W. Tam, and S. R. Marder for information in advance of publication.